

# **Step-wise modifications Influence of modifications (from AoB2015 to v0.5) in the Vegetation Optimality Model**

Remko C. Nijzink<sup>1</sup>, Jason Beringer<sup>2</sup>, Lindsay B. Hutley<sup>3</sup>, and Stanislaus J. Schymanski<sup>1</sup>

<sup>1</sup>Luxembourg Institute of Science and Technology, Environmental Research and Innovation, Catchment and Eco-hydrology Research Group, Belvaux, Luxembourg

<sup>2</sup>School of Agriculture and Environment, The University of Western Australia, Crawley, WA, Australia, 6909

<sup>3</sup>Research Institute for the Environment and Livelihoods, Charles Darwin University, Darwin, NT, Australia, 0909

**Correspondence:** R.C. Nijzink (remko.nijzink@list.lu)

## **Abstract.**

The Vegetation Optimality Model (VOM, Schymanski et al., 2009, 2015) is an optimality-based, coupled water-vegetation model that predicts vegetation properties and behaviour based on optimality theory, rather than calibrating vegetation properties or prescribing them based on observations, as most conventional models do. ~~In order to determine Several updates to previous~~

~~5 applications of the VOM have been made for the study in the accompanying paper of Nijzink et al. (2021), where we assess~~ whether optimality theory can alleviate common shortcomings of conventional models, as identified in a previous model inter-comparison study along the North Australian Tropical Transect (NATT) (Whitley et al., 2016), ~~a range of updates to previous~~ ~~applications of the VOM have been made for increased generality and improved comparability with conventional models. To~~ ~~assess in how far. Therefore, we assess in this technical paper how~~ the updates to the model and input data would have affected ~~10 the original results, and~~ we implemented them ~~one-by-one one at a time~~ while reproducing the analysis of Schymanski et al. (2015).

The model updates included extended input data, the use of variable atmospheric CO<sub>2</sub>-levels, modified soil properties, implementation of free drainage conditions, and the addition of grass rooting depths to the optimized vegetation properties. A systematic assessment of these changes was carried out by adding each individual modification to the original version of the ~~15~~ VOM at the flux tower site of Howard Springs, Australia.

The analysis revealed that the implemented changes affected the simulation of mean annual evapo-transpiration (ET) and gross primary productivity (GPP) by no more than 20%, with the largest effects caused by the newly imposed free drainage conditions and modified soil texture. Free drainage conditions led to an underestimation of ET and GPP, whereas more fine-grained soil textures increased the water storage in the soil and resulted in increased GPP. Although part of the effect of free ~~20~~ drainage was compensated for by the updated soil texture, when combining all changes, the resulting effect on the simulated fluxes was still dominated by the effect of implementing free drainage conditions. Eventually, the relative error for the mean annual ET, in comparison with flux tower observations, changed from an 8.4% overestimation to an 10.2% underestimation, whereas the relative errors for the mean annual GPP stayed similar with a change from 17.8% to 14.7%. The sensitivity to free drainage conditions suggests that a realistic representation of groundwater dynamics is very important for predicting ET and

25 GPP at a tropical open-forest savanna site as investigated here. The modest changes in model outputs highlighted the robustness of the optimization approach that is central to the VOM architecture.

## 1 Introduction

Novel modelling approaches that are able to explicitly model vegetation dynamics, such as vegetation cover or root surfaces, may lead to an overall improved understanding of carbon and water flux exchanges with the atmosphere. Recent model inter-comparison studies also reveal that novel model approaches are needed, especially related to vegetation dynamics (e.g. Whitley et al., 2016). Therefore, we use here optimality theory to predict models with explicit vegetation dynamics are needed (Whitley et al., 2016). Optimality theory predicts the variation and dynamics of vegetation cover, root systems, water use and carbon uptake without the need for site-specific input about vegetation properties, by optimizing these properties for a certain objective, such as maximizing the carbon gain by photosynthesis (Hikosaka, 2003; Raupach, 2005; Buckley and Roberts, 2006) or minimizing water stress (Rodríguez-Iturbe et al., 1999; Rodríguez-Iturbe et al., 1999). The theory used here is based on the premise that the net carbon profit (NCP) Net Carbon Profit (NCP, Schymanski et al., 2007, 2008a, 2009), which is the difference between carbon assimilated by photosynthesis and carbon expended on construction and maintenance of all the plant tissues needed for photosynthesis and water uptake and storage, is an appropriate measure of plant fitness, given that assimilated carbon is a fundamental resource of plant growth, development, survival and reproduction. The theory further assumes that construction and maintenance costs of plant organ functionality are general and therefore transferable between species and sites. Hence, the costs and benefits at different sites are determined in a consistent way, leading to vegetation properties that solely depend on physical conditions, such as meteorological forcing, soils and hydrology. As a result, this leads to a systematic and consistent explanation of vegetation behaviour under different external conditions at different sites.

These optimality principles were employed in the Vegetation Optimality Model (VOM, Schymanski et al., 2009, 2015).  
45 The VOM is a coupled water-vegetation model that optimizes vegetation properties to maximize the Net Carbon Profit (NCP) → NCP in the long-term (20-30 years) for given climate and physical properties at the site under consideration. The NCP is defined as the difference between the total carbon amount assimilated by photosynthesis, and the total carbon costs for the maintenance of leaf area, photosynthetic capacity and root surface area, as described in Schymanski et al. (2007, 2008b). The VOM has been previously applied by Schymanski et al. (2009) and Schymanski et al. (2015) at Howard Springs, a  
50 flux tower site in the North Australian Tropical Transect (NATT, Hutley et al., 2011). The NATT consists of multiple flux tower sites along a precipitation gradient from north to south, which allows for a more systematic testing of the VOM under different climatological circumstances. The NATT has been used previously in an intercomparison of terrestrial biosphere models (TBMs) by Whitley et al. (2016), which revealed that lacking or wrong vegetation dynamics and incorrect assumptions about rooting depths have a strong influence on the performance of state-of-the-art TBMs. Previous studies show that rooting  
55 depths vary considerably with precipitation (Schenk and Jackson, 2002) and, thus, also along the North Australian Tropical Transect (Williams et al., 1996; Ma et al., 2013). In contrast to these TBMs, the VOM predicts rooting depths and vegetation dynamics, and provides therefore a novel approach for the simulation of these savanna sites. In order to find out if this novel

approach can help to overcome the shortcomings of common TBMs, in the accompanying paper by Nijzink et al. (2021) the VOM was applied to the same sites along the NATT and systematically compared with the previous simulations presented by Whitley et al. (2016).

To assess in how far the In order to understand if predicted optimality-based simulation of rooting depths, tree cover and vegetation dynamics may alleviate the shortcomings of TBMs identified by Whitley et al. (2016), we propose to run the VOM using rooting depths and vegetation cover result in better simulations. Nijzink et al. (2021) ran the VOM both with predicted and prescribed rooting depths and vegetation cover while systematically comparing simulated fluxes with observations and the output of the other TBMs. For that reason, Nijzink et al. (2021) made several changes to the VOM set-up of Schymanski et al. (2015) in order to use the same input data and similar physical boundary conditions at the different sites as the TBMs in Whitley et al. (2016). In the In the remainder of this paper, the new set-up in Nijzink et al. (2021) will be referred to as VOM-v0.5, in contrast to VOM-AoB2015 for the set-up of Schymanski et al. (2015).

First, in the simulations by Whitley et al. (2016), all TBMs were run under the assumption of a freely draining soil column, even though studies suggest an influence of groundwater on the resulting fluxes (York et al., 2002; Bierkens and van den Hurk, 2007; Max... Free draining conditions can be mimicked in the VOM by setting drainage parameters to very fast drainage and the critical water table for the onset of drainage very low (see below). In contrast, the VOM-AoB2015 used a hydrological schematization based on the local topography around the flux tower site (Schymanski et al., 2008b), which resulted in groundwater tables varying around 5 m below the surface. For better comparability with Whitley et al. (2016), the boundary conditions of the VOM were adjusted to resemble freely draining conditions. Assessment of the influence of this change could lead to additional insights about the influence of groundwater on the resulting carbon and water fluxes, which can be significant (York et al., 2002; Bierkens and van den Hurk, 2007).

In previous applications of the VOM (Schymanski et al., 2009, 2015), Another modification concerns the prescribed atmospheric CO<sub>2</sub>concentrations were assumed constant concentrations. The VOM-AoB2015 assumed constant atmospheric CO<sub>2</sub>-concentrations over the entire modelling period, whereas for inter-comparison with other models, we should use the VOM-v0.5 used measured CO<sub>2</sub>-levels-concentrations, which have increased considerably over the past years (Keeling et al., 2005). Previous applications of the VOM also prescribed a The previously documented influence of atmospheric CO<sub>2</sub>-concentrations on the water and carbon fluxes simulated by the VOM (Schymanski et al., 2015) calls for a systematic assessment of this change.

In the VOM-AoB2015, the grass rooting depth was prescribed to a value of 1 m, arguing that only tree roots could penetrate into deeper layers due to the presence of a hard pan at Howard Springs, only tree roots could penetrate into deeper layers. Since we do not know if such features exist which not necessarily exists at the other sites along the NATT, rooting depth of seasonal vegetation should be optimised in a similar way as that of perennial vegetation. In order to make the VOM applicable to all sites along the NATT, the grass rooting depth was not prescribed but also optimized for NCP in the VOM-v0.5, but an evaluation of the effect of this change on the original simulations was not included in Nijzink et al. (2021).

In addition to the changes in the boundary conditions, model code and parametrization mentioned above, higher computational power, allowing for finer discretizations, and updated forcing data may also affect simulation results. In general, reproducing

benchmark datasets is often seen as necessary in order to be confident about the model and the numerical implementation (Blyth et al., 2011; Abramowitz, 2012; Clark et al., 2021). Here we argue that it is also important to assess effects of individual changes one at a time, to avoid obtaining "the right results for the wrong reasons" as two errors may compensate for each other when comparing the final results with a given benchmark.

Therefore, we assess to what extent the various changes influence the VOM-results, a new set-up of the VOM was applied to the by adding these changes one at a time to the VOM-AoB2015, for the same flux tower site in Australia, Howard Springs, as in Schymanski et al. (2009, 2015). This technical note describes the nine changes to the VOM since its last application by Schymanski et al. (2015), and how they affect the results of the VOM one-by-one individually and in combination. In this way, this work should point at important model decisions and sensitivities of the VOM, as well as TBMs in general. At the same time, this work showcases a systematic evaluation of model updates and changes, which we deem necessary in model applications.

## 2 Methodology

All steps in the process, from pre- and post-processing to model runs, were done in an open science approach using the RENKU<sup>1</sup> platform. The workflows including code and input data can be found online<sup>2</sup>. In the following, we briefly describe the study site, the VOM, and the various modifications done in this study, compared to Schymanski et al. (2015).

### 2.1 Study site

The study site used by Schymanski et al. (2009) and Schymanski et al. (2015) is Howard Springs (How-AU-AU-How), which was previously used by Schymanski et al. (2009) and Schymanski et al. (2015) and therefore used in this analysis as well. At the same time, the flux tower site at Howard Springs provides a long record of carbon dioxide and water fluxes starting from 2001 (Berenger et al., 2016). Howard Springs is the wettest site (with an average precipitation of 1747 mm/year (SILO Data Drill, Jeffrey et al., 2001, calculated for 1980-2017) along the North Australian Tropical Transect (NATT, Hutley et al., 2011), which has a strong precipitation gradient from north to south, with a mean annual precipitation around 500 mm/year at the driest site. The vegetation at Howard Springs consists of a mostly evergreen overstorey (mainly *Eucalyptus miniata* and *Eucalyptus tetrodonta*) and an understorey dominated by annual *Sorghum* and *Heteropogon* grasses. The soils at Howard Springs are well-drained red and grey kandosols, and have a high gravel content and a sandy loam structure.

### 2.2 Vegetation Optimality Model

The Vegetation Optimality Model (VOM, Schymanski et al., 2009, 2015) is a coupled water and vegetation model, that optimizes vegetation properties by maximizing the Net Carbon Profit NCP. The model code and documentation can be found on

<sup>1</sup><https://renkulab.io/>

<sup>2</sup><https://renkulab.io/gitlab/remko.nijzink/vomcases>

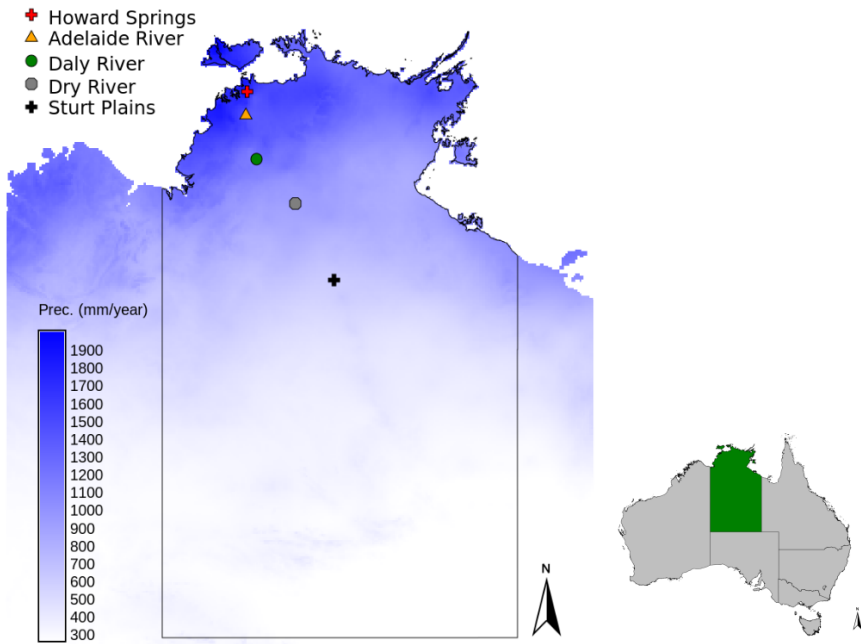


**Figure 1.** Location of the Howard Springs site, together with the other flux tower sites that are part of the North Australian Tropical Transect in the Northern Territory of Australia, with the mean annual precipitation shown in the blue colorscale (SILO Data Drill, Jeffrey et al., 2001, calculated for 1980-2017).

line<sup>3</sup>,<sup>4</sup> and version v0.5<sup>5</sup> of the model was used here. A general description is given below, whereas a more detailed description The processes and parameterizations are not modified in the VOM-v0.5, unless explicitly stated in Sect. 2.2.9. Therefore, more details of the VOM can be found at Schymanski et al. (2009, 2015) in Schymanski et al. (2009, 2015), whereas detailed descriptions about the root processes can be found in Schymanski et al. (2008b) and the canopy processes in Schymanski et al. (2007)

125 . Nevertheless, a general description of the VOM is given below for completeness.

### 2.2.1 Vegetation model

The VOM schematizes the ecosystem as two big leaves (see also Figure 2), one representing the seasonal vegetation (grasses) and one representing the perennial vegetation (trees). Photosynthesis was modelled according to Schymanski et al. (2007), who simplified the of both the seasonal and perennial vegetation was modelled with a simplified canopy-gas exchange model of von 130 Caemmerer (2000) for C<sub>3</sub>-plants. This was done by Schymanski et al. (2009) for a greater generality of the VOM, even though it may not correctly represent photosynthesis of the C<sub>4</sub>-grasses at the site. The model computes CO<sub>2</sub>-uptake as a function

<sup>3</sup><https://github.com/schymans/VOM>

<sup>4</sup><https://vom.readthedocs.io>

<sup>5</sup><https://doi.org/10.5281/zenodo.3630081>

**Table 1.** Characteristics of the Howard Springs site. Vegetation data from Hutley et al. (2011), Hutley (2015) and Whitley et al. (2016), with Eucalyptus (Eu.), Erythrophleum (Er.), Hetropogon (He.). Meteorological data is taken from the SILO Data Drill (Jeffrey et al., 2001) for the model periods of 1-1-1980 until 31-12-2017, with the ~~potential evaporation reference crop evapotranspiration~~ calculated according to the FAO Penman-Monteith formula (Allen et al., 1998). The ratio of the net radiation  $Rn$  with the latent heat of vaporization  $\lambda$  multiplied with the precipitation  $P$ , is defined here as the aridity  $Rn/\lambda P$ . Tree cover is determined as the minimum value of the mean monthly projective cover based on fPAR-observations (Donohue et al., 2013). The maximum grass cover was found by subtracting the tree cover from the remotely sensed projective cover.

Study Site	Howard Springs
FLUXNET ID	AU-How
Coordinates	12.49S 131.35E
<del>Precipitation</del> (mm year $^{-1}$ )	1747
<del>Pot. evap–Ref. crop evapotranspiration</del> (mm year $^{-1}$ )	1763
Aridity $\div(-)$	1.03
Net <del>Rad.</del> <del>Radiation</del> (MJ m $^{-2}$ year $^{-1-1-1}$ )	4392
Mean <del>max–maximum</del> temp. [°C]	37.5
Mean <del>min–minimum</del> temp. [°C]	27.4
Tree cover (%)	39.8
<del>Max–Maximum</del> grass cover (%)	44.3
Species	
Overstorey	<i>Eu. miniata</i> <i>Eu. tetrodonta</i> <i>Er. chlorostachys</i>
Understorey	<i>Sorghum spp.</i> <i>He. triticeus</i>

of irradiance, atmospheric CO<sub>2</sub>-concentrations, ~~temperature, photosynthetic capacity, projected foliage cover photosynthetic capacity and stomatal conductance:~~

$$A_g = \frac{1}{8} \left( 4C_a G_s + 8\Gamma_* G_s + \left( (J_e - 4R_l - 4G_s(C_a - 2\Gamma_*))^2 + 16G_s(8C_a G_s + J_e + 8R_l)\Gamma_* \right)^{\frac{1}{2}} \right) \quad (1)$$

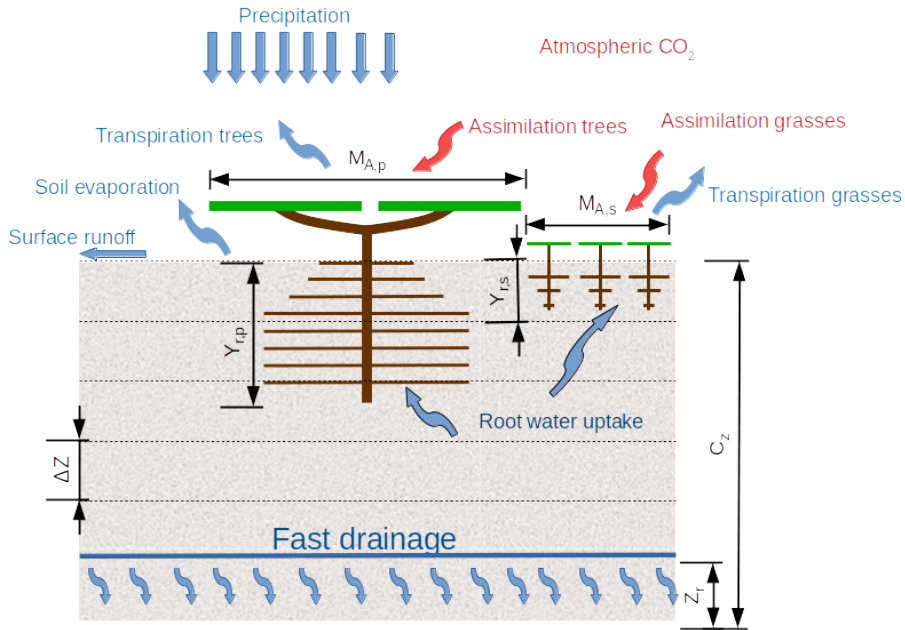


**Figure 2.** Schematization of the Vegetation Optimality Model as two big leaves, with  $M_{A,p}$  and  $M_{A,s}$  the fractional cover of perennial trees and seasonal grasses respectively,  $y_{r,p}$  and  $y_{r,s}$  the rooting depths of the perennial trees and seasonal grasses respectively,  $\Delta Z$  the soil layer thickness,  $C_Z$  the total soil depth, and  $Z_r$  the drainage depth.

135 with  $J_e$  the electron transport rate ( $\text{mol m}^{-2} \text{ s}^{-1}$ ),  $G_s$  stomatal conductance ( $\text{mol m}^{-2} \text{ s}^{-1}$ ),  $R_l$  leaf respiration ( $\text{mol m}^{-2} \text{ s}^{-1}$ ),  $C_a$  the mol fraction of  $\text{CO}_2$  in the air and  $\Gamma_*$  the  $\text{CO}_2$  compensation point ( $\text{mol CO}_2 \text{ mol}^{-1} \text{ air}$ ). The electron transport rate  $J_e$  was calculated as:

$$J_e = \left( 1.0 - e^{\frac{0.3 I_a}{J_{max}}} \right) \cdot J_{max} \cdot M_a \quad (2)$$

140 with  $I_a$  the irradiance ( $\text{mol m}^{-2} \text{ s}^{-1}$ ),  $J_{max}$  the electron transport capacity ( $\text{mol m}^{-2} \text{ s}^{-1}$ ) and  $M_a$  the projected cover of vegetation (dimensionless fraction). The leaf respiration  $R_l$ , as used in Equation 1, is defined as:

$$R_l = \frac{M_a \cdot c_{Rl} \cdot J_{max} \cdot (C_a - \Gamma_*)}{8 \cdot (C_a + 2 \cdot \Gamma_*)} \quad (3)$$

with  $c_{RL}$  a constant set to 0.07 (dimensionless), based on Schymanski et al. (2007). The electron transport capacity  $J_{max}$  in Equations 2 and 3 is determined in the following way:

$$J_{max} = \frac{J_{max,25} \left( h_a \left( e^{-\frac{h_d(T_{opt}-298.0)}{273T_{opt}R+25.0}} - 1.0 \right) + h_d \right) e^{\frac{h_a(T_a-25.0)(273.0T_{opt}R+T_{opt}-273.0)}{(T_a+273.0T_{opt}R)(273.0T_{opt}R+25.0)}}}{h_a \left( e^{\frac{h_d(T_a-T_{opt}+273.0)}{T_a+273.0T_{opt}R}} - 1.0 \right) + h_d} \quad (4)$$

145 with  $h_a$  and stomatal conductance, whereby photosynthetic capacity,  $h_d$  two parameters set to 43.79 and 200  $\text{kJ mol}^{-1}$  respectively (values taken for *Eucalyptus pauciflora*, see Schymanski et al., 2007), the electron transport capacity at 25 °C  $J_{max,25}$  ( $\text{mol m}^{-2} \text{ s}^{-1}$ ) and the optimal temperature  $T_{opt}$  (K), set to the mean monthly daytime temperature at the site (305 K, Schymanski et al., 2007). In the equations above, the electron transport capacity at 25 °C  $J_{max,25}$ , the projected foliage cover  $M_a$  and stomatal conductance  $G_s$  are optimized dynamically in a way to maximize the overall Net Carbon Profit (NCP) of the vegetation over the entire simulation period. Optimization is possible due to the carbon costs associated with each of these variables: photosynthetic capacity is linked to maintenance respiration, projected cover to the is linked to foliage turnover and maintenance of leaf area costs, while stomatal conductance is linked to transpiration (depending on the atmospheric vapour pressure deficit) and hence root water uptake costs and limitations. Root water uptake is modelled following an electrical circuit analogy, where the water potential difference between the plant and each soil layer drives the flow. Here, :

$$155 \quad Q_{r,i} = S_{A,r} \frac{h_{r,i} - h_i}{\Omega_r + \Omega_{s,i}} \quad (5)$$

with  $S_{A,r}$  the root surface area and soil hydraulic conductivity in each soil layer determine the resistance (Schymanski et al., 2008b) ( $\text{m}^2 \text{ m}^{-2}$ ),  $h_{r,i}$  the hydraulic head in the roots (m),  $h_i$  the hydraulic head in the soil (m),  $\Omega_r$  the radial root resistivity (s) and  $\Omega_{s,i}$  the soil resistivity (s), with subscript  $i$  denoting the specific soil layer. The root surface area, in return, generates carbon costs for maintenance and the vertical distribution in the soil profile  $S_{A,r}$  is optimized in a way to satisfy the canopy water demand with the minimum possible total root surface area.

## 2.2.2 Long-term optimization

The rooting depths of the perennial trees and the seasonal grasses ( $y_{r,p}$  and  $y_{r,s}$ ) as well as the foliage projected cover of the perennial vegetation ( $M_{A,p}$ ) are derived by optimizing these properties for the long-term, assuming that these do not vary significantly during the simulation period (20-30 years). Similarly, water use strategies of both the perennial and the seasonal vegetation component components are assumed to be a result of long-term natural selection for a given site, and are also optimized in order to maximize the Net Carbon Profit NCP. To do so, the water use strategy was expressed as a functional relation between the marginal water cost of assimilation (Cowan and Farquhar, 1977), represented by  $\lambda_p$  and  $\lambda_s$  ( $\text{mol mol}^{-1}$ )

$\text{m}^{-1}$ ) for perennial and seasonal vegetation respectively, and the sum of water suction heads ( $h_i$ ) in all soil layers within the root zone, ~~after Schymanski et al. (2009)~~:

$$170 \quad \lambda_s = c_{\lambda f, s} \left( \sum_{i=1}^{i_{r,s}} h_i \right)^{c_{\lambda e, s}} \quad (6)$$

$$\lambda_p = c_{\lambda f, p} \left( \sum_{i=1}^{i_{r,p}} h_i \right)^{c_{\lambda e, p}} \quad (7)$$

where  $c_{\lambda f, s}$  ( $\text{mol mol}^{-1} \text{m}^{-1}$ ),  $c_{\lambda e, s}$  (-),  $c_{\lambda f, p}$  ( $\text{mol mol}^{-1} \text{m}^{-1}$ ) and  $c_{\lambda e, p}$  (-) are the optimized parameters, while  $i_{r,p}$  and  $i_{r,s}$  represent the number of soil layers reached by perennial and seasonal roots, respectively. ~~Note that Cowan and Farquhar (1977) proposed that  $\lambda$  should decline with declining soil water content, whereas Schymanski et al. (2009) argued that plants more likely sense the soil suction head than the total available water. Equations 6 and 7 formulated  $\lambda$  as an explicit but flexible function of the average suction head in the root zone, where the shape of the function (determined by the two optimized parameters) represents a specific water use strategy.~~

After the establishment of the optimized water use parameters in Eqs. 6 and 7 (~~i.e. the long-term relation between soil water marginal water costs~~), the values of  $\lambda_p$  and  $\lambda_s$  are calculated for each day separately and then used to simulate the 180 diurnal variation in stomatal conductance using Cowan-Farquhar optimality (Cowan and Farquhar, 1977; Schymanski et al., 2008a). The values of  $c_{\lambda f, s}$ ,  $c_{\lambda e, s}$ ,  $c_{\lambda f, p}$  and  $c_{\lambda e, p}$  ~~essentially~~ express how quickly plants reduce water use as soil water suction increases during dry periods. The ~~slower  $\lambda_s$  and  $\lambda_p$  are reduced in response to drying soil, the larger the root costs are as the root systems are adjusted to satisfy the canopy water demand. The~~ parameters ( $c_{\lambda f, s}$ ,  $c_{\lambda e, s}$ ,  $c_{\lambda f, p}$  and  $c_{\lambda e, p}$ ) are optimized and constant in the long-term, along with  $y_r$  and  $M_{A,p}$ , to maximize the total NCP over the entire simulation period.

### 185 2.2.3 Short-term optimization

Some vegetation properties, such as seasonal vegetation cover ( $M_{A,s}$ ), ~~photosynthetic capacities~~ the electron transport capacities at 25 °C for the seasonal and perennial vegetation ( $J_{max25,p}$  and  $J_{max25,s}$ ) and root surface area distributions of the seasonal and perennial vegetation component ( $S_{Adri,s}$  and  $S_{Adri,p}$ ), are allowed to vary on a daily basis to reflect their dynamic nature. ~~Their values are hence~~ Here, the root surface area distributions are optimized day by day in a way to satisfy the canopy water demand. The other vegetation properties are optimized from day to day in a way to maximize the daily NCP. This is done by using three different values for each of these vegetation properties, the actual value and a specific increment above and below this value every day, and at the end of the ~~simulated~~ day the combination of values that would have achieved the maximum NCP on the present day is selected for the next day. ~~See Schymanski et al. (2009, 2015) for details~~ These vegetation parameters always vary on a daily basis, even though the time step of the VOM is usually hourly or sub-hourly. Only the stomatal conductances, as determined by Cowan-Farquhar optimality, are varied over an hourly time step.

## 2.2.4 Carbon cost functions

As mentioned above, different carbon cost functions are used to quantify the maintenance costs for different plant organs. The carbon cost related to foliage maintenance is based on a linear relation between the total leaf area and a constant leaf turnover cost factor:

200 
$$R_f = L_{AIc} \cdot c_{tc} \cdot M_{A,p} \quad (8)$$

where  $L_{AIc}$  is the clumped leaf area (set to 2.5 (Sehymanski et al., 2007)),  $c_{tc}$  is the leaf turnover cost factor (set to 0.22  $\mu\text{mol}^{-1} \text{s}^{-1} \text{m}^{-2}$ , (Sehymanski et al., 2007)) and  $M_{A,p}$  is the perennial vegetation cover fraction.

The costs for root maintenance were defined as (Sehymanski et al., 2008b):

$$R_r = c_{Rr} \cdot \left( \frac{r_r}{2} \cdot S_{A,r} \right) \quad (9)$$

205 where  $c_{Rr}$  is the respiration rate per fine root volume ( $0.0017 \text{ mol s}^{-1} \text{ m}^{-3}$ ),  $r_r$  the root radius (set to  $0.3 \cdot 10^{-3} \text{ m}$ ) and which were both derived by Schymanski et al. (2008b) from experimental data on citrus plants. Here, we present a sensitivity analysis of these parameters in Supplement S5.  $S_{A,r}$  represents the root surface area per unit ground area ( $\text{m}^2 \text{m}^{-2}$ ). The values used in this parameterization stem from observations on citrus plants, as described by Schymanski et al. (2008b).

Water transport costs are assumed to depend on the size of the transport system, from fine roots to the leaves. The canopy 210 height is not modelled in the VOM, and the transport costs are therefore just a function of rooting depth and vegetated cover:

$$R_v = c_{rv} \cdot M_A \cdot y_r \quad (10)$$

where  $c_{rv}$  is the cost factor for water transport ( $\text{mol m}^{-3} \text{ s}^{-1}$ ),  $M_A$  the fraction of vegetation cover (–), and  $y_r$  the rooting depth (m). The cost factor  $c_{rv}$  was set to  $1.0 \mu\text{mol m}^{-3} \text{ s}^{-1}$  by Schymanski et al. (2015) after a sensitivity analysis for Howard Springs, which is also adopted here.

## 215 2.2.5 Water balance model

As described in Sehymanski et al. (2015), the The soil is schematized as a permeable block containing an unsaturated zone and a saturated zone (see also Figure 2), overlaying an impermeable bedrock with a prescribed drainage level. The model simulates a variable water table based on the vertical fluxes between horizontal soil layers and a drainage flux computed as a function of the water table elevation. Here, the thickness of soil layers was prescribed to 0.2 m, based on a sensitivity analysis 220 for Howard Springs, see also Supplement S2. The vertical fluxes between soil layers are determined using a discretization of the Buckingham-Darcy equation (Radcliffe and Rasmussen, 2002), resulting in the 1-D Richards' equation of steady flow. The matric suction heads and unsaturated conductivities were determined with the model of Van Genuchten (1980).

The hydrological parameters that determine the drainage outflow and groundwater tables are a hydrological length scale for seepage outflow, channel slope and drainage level  $z_r$ , as defined by Schymanski et al. (2015) and based on Reggiani et al. 225 (2000). The seepage outflow is determined by the elevation difference between groundwater table and drainage level, divided by a resistance term that uses the hydrological length scale and channel slope (Eq. 10, Schymanski et al., 2008b). Originally, the hydrological length scale and channel slope were adopted from Reggiani et al. (2000) and set to 10 m and 0.033 rad, respectively, in absence of more detailed knowledge about these parameters. At the same time, Schymanski et al. (2015) set the drainage level  $z_r$  and total soil thickness  $c_z$  to 10 m and 15 m, respectively, based on the local topography around the flux 230 tower site (Schymanski et al., 2008b). This hydrological schematization resulted in groundwater tables around 5 m below the surface.:

Here, the hydrological parameters were set in a way to resemble freely draining conditions, i.e. avoiding a significant influence of groundwater in Figure 2, for consistency with other model applications (e.g. Whitley et al., 2016), with a total soil thickness  $c_z$

$$235 \quad Q_{s,f} = K_{sat} \cdot \frac{\omega_0 \cdot (y_s - z_r)}{2 \cdot \cos(\gamma_0) \cdot \Lambda_s} \quad (11)$$

with  $\gamma_0$  the average slope of 30 m, a fast drainage parameterization with a drainage level the seepage face (rad),  $\Lambda_s$  a hydrological length scale (m),  $y_s$  the groundwater table (m),  $K_{sat}$  the saturated hydraulic conductivity ( $\text{m s}^{-1}$ ),  $\omega_0$  the saturated surface area fraction and  $z_r$  of 5 m, a length scale for seepage outflow set to 2 m and a channel slope set to 0.02 rad. the drainage level (m).

240 As illustrated in Figure 2, when precipitation falls on this soil block, it either causes immediate surface runoff or infiltrates. Once infiltrated, it can be taken up by roots and transpired, or it can evaporate at the soil surface, or move downwards until it drains away at a depth of 30 m, well below the rooting zone (i.e. parameterized to represent freely draining conditions for comparison with other models). The simulation of soil evaporation and vertical fluxes in the unsaturated zone are described in Schymanski et al. (2008b, 2015) defined by the drainage level  $z_r$  and total soil thickness  $c_z$ . In the top soil layer, soil evaporation 245 is determined as a function of the soil moisture, global radiation and vegetation cover.

## 2.2.6 Model optimization

The VOM uses the Shuffled Complex Evolution algorithm (SCE, Duan et al., 1994) to optimize the vegetation properties listed in Table 3 for maximum Net Carbon Profit (NCP) NCP over the entire simulation period (37 years for the new VOM set-up VOM-v0.5, from 1-1-1980 until 31-12-2017). The SCE-algorithm uses first an initial random seed, subdivides the parameter sets into complexes and performs a combination of local optimization within each complex and mixing between complexes to converge to a global optimum. Here, we set the initial number of complexes to 10. The VOM uses a variable time step, where the target time step length of 1 hour is reduced if any state variable in the model changes by more than 10% per time step.

### 2.2.7 Model input and Meteorological data

A relatively long timeseries of meteorological inputs is required to run and optimize the VOM. For this reason, Schymanski et al. (2015)

255 used data from the Australian SILO Data Drill (Jeffrey et al., 2001), from which a newer version was applied to the new VOM set-up. The necessary meteorological data includes daily time series of daily maximum and minimum temperatures, short-wave radiation, precipitation, vapour pressure and atmospheric pressure. Atmospheric, which were taken from the Australian SILO Data Drill (Jeffrey et al., 2001). In addition, the VOM requires information about atmospheric CO<sub>2</sub>-levels were originally assumed constant by Schymanski et al. (2015), but in the new set-up, these were taken from, which were provided as a constant 260 in the VOM-AoB2015 version, whereas for the VOM-v0.5 used here, we used the Mauna Loa CO<sub>2</sub>-records (Keeling et al., 2005), see also Sect. 2.2.9. Eventually, these daily time series are converted in the VOM to hourly time series, as described by Schymanski et al. (2009).

Observed atmospheric CO<sub>2</sub>-levels at the flux tower were not used due to the required length of the timeseries for the VOM (20-30 years). The measured meteorological variables at the flux tower sites were only used to verify the SILO meteorological 265 data, which revealed only minor differences in the resulting fluxes of the VOM when the SILO-data was replaced for the days that flux tower observations were available (max. 6%, see Figure S4.3 in Supplement S4). See also Supplement S3, Figure S3.1 for the time series of meteorological data.

270 The soils, originally assumed vertically homogeneous by Schymanski et al. (2015), were parameterized based on field measurements of sand, clay and silt content provided by L. B. Hutley and J. Beringer in the top 10 cm, and the Soil and Landscape Grid of Australia (Viscarra Rossel et al., 2014a,b,c) for the deeper layers. The soils were classified into one of the soil textural groups of Carsel and Parrish (1988) based on the fractions of sand, silt and clay. Eventually, the parameters for the soil water retention model of Van Genuchten (1980) and the hydraulic conductivity were taken from the accompanying tables<sup>6</sup> from Carsel and Parrish (1988). See also Table 2 for the soil parameterization.

### 2.2.8 Model evaluation data

275 At Howard Springs, a flux tower that is part of the regional FLUXNET network OzFlux (Beringer et al., 2016), provides time series of net ecosystem exchange (NEE) of carbon dioxide and latent heat flux (LE) for model evaluation. The Dingo-algorithm (Beringer et al., 2017) was applied to the data for a gap-filled estimation of gross primary productivity (GPP) and latent heat flux (LE). LE was converted to evapo-transpiration (ET), defined here as the sum of all evaporation and transpiration processes, even though these processes are different in nature (Savenije, 2004). Eventually, the gap-filled observations of GPP 280 and ET were compared with the modelled fluxes. The original model application of Schymanski et al. (2015) was run until 31-12-2005, and VOM-AoB2015 was originally run until the end of 2005, and for this reason, the modelled fluxes were for that reason evaluated for the overlapping period between model and flux tower observations from 07-08-2001 until 31-12-2005. For consistency, the new VOM-VOM-v0.5 runs were evaluated for the same time period.

<sup>6</sup>see also <https://vom.readthedocs.io/en/latest/soildata.html>

**Table 2.** Vertical profile of soil characteristics at Howard Springs, based on data from the Soil and Landscape Grid of Australia (Viscarra Rossel et al., 2014a,b,c), in addition to field measurements of J. Beringer and L. B. Hutley. Here,  $\theta_r$  refers to the residual moisture content,  $\theta_s$  the saturated water content,  $\alpha$  and  $n$  the Van Genuchten soil parameters (Van Genuchten, 1980) and  $K_{sat}$  the saturated hydraulic conductivity.

Howard Springs	Soil type	$\theta_r$ (-)	$\theta_s$ (-)	$\alpha$ (1/m)	$n$ (-)	$K_{sat}$ (m/s)
0.00-0.20m	Sandy Loam	0.065	0.41	7.5	1.89	$1.228 * 10^{-5}$
0.20-0.40m	Sandy Loam	0.065	0.41	7.5	1.89	$1.228 * 10^{-5}$
0.40-0.60m	Sandy Clay Loam	0.1	0.39	5.9	1.48	$3.639 * 10^{-6}$
0.60-bedrock	Sandy Clay Loam	0.1	0.39	5.9	1.48	$3.639 * 10^{-6}$

To evaluate the foliage projected cover (FPC) dynamics of seasonal and perennial vegetation predicted by the VOM, defined as the sum of  $M_{A,p}$  and  $M_{A,s}$  we used satellite-derived monthly fractions of Photosynthetically Active Radiation absorbed by vegetation (fPAR) from Donohue et al. (2008, 2013), which were converted into estimates of FPC. The maximum possible value of fPAR was defined as 0.95 by Donohue et al. (2008) and relates to maximum projective cover (i.e. FPC = 1.0). The linear relation of FPC with fPAR-data (Asrar et al., 1984; Lu, 2003) allowed for the calculation of FPC by dividing the fPAR-values by the maximum value of 0.95.

## 290 2.2.9 Modifications Systematic analysis of modifications to the VOM set-up

In comparison with previous applications of the VOM (Sehymanski et al., 2009, 2015), several changes were made regarding the input data and process representation. Each individual change was added to the reference set-up of Sehymanski et al. (2015) to assess the sensitivity of the model results for that change the VOM-AoB2015 (see also Supplement S1). Briefly, the changes were assessed by the following cases We define here 12 model cases, including the 9 changes to the VOM-AoB2015, the reproduction of the VOM-AoB2015, the re-optimization of the VOM-AoB2015 and the final VOM-v0.5 (see also Table 4):

- Reproduction 1. Reproduction of the results of (Sehymanski et al., 2015): the VOM Schymanski et al. (2015)

The model code of the VOM-v0.5 was run with the same vegetation parameters and input data as (Sehymanski et al., 2015), in order to check the new version of the VOM code for reproducibility the VOM-AoB2015. The model was run from

300 1-1-1976 until 31-12-2005. This was done in order to check the reproducibility of the results of Schymanski et al. (2015)

~

- 2. Re-run SCE : the

The VOM was re-optimized with the same settings and input data as (Sehymanski et al., 2015), in order to assess whether the optimization algorithm converges to the same results as (Sehymanski et al., 2015). The model was run the

VOM-AoB2015, and run with the same model period from 1-1-1976 until 31-12-2005. Also here, the specific goal was to  
reproduce the results of Schymanski et al. (2015), as the optimization algorithm should converge to the same solutions.

– 3. Variable CO<sub>2</sub>-levels ~~instead of using static atmospheric~~

Atmospheric CO<sub>2</sub>-levels were originally assumed constant in the VOM-AoB2015 with CO<sub>2</sub>-concentrations of 350 ppm,  
the CO<sub>2</sub>-concentrations ~~but in the VOM-v0.5, these were taken~~ from the Mauna Loa CO<sub>2</sub>-records (Keeling et al.,  
310 ~~2005) were used in the new model runs. The model was optimized here.~~ Therefore, the VOM-AoB2015 was run with  
variable CO<sub>2</sub>-levels, and optimized for the period 1-1-1976 until 31-12-2005. This was done in order to assess the  
sensitivity of the model to variable CO<sub>2</sub>-levels.

– 4. Reduced soil layer thickness ~~the~~

The soil layer thickness was set to 0.2 m, instead of the 0.5 m used by Schymanski et al. (2015) in the VOM-AoB2015,  
315 after running a sensitivity analyses with the VOM-v0.5 (see also Supplement S2). The model was optimized here  
VOM-AoB2015 was also run with 0.2 m now, and optimized for the period 1-1-1976 until 31-12-2005, in order to  
assess the influence of different soil layer thicknesses on the VOM-AoB2015 results.

– 5. Variable atmospheric pressure ~~a~~

A new version of the meteorological data from the Australian SILO Data Drill (Jeffrey et al., 2001) provided time series  
320 of atmospheric pressure starting from 1-1-1980, whereas originally this had been fixed at a level of 1013 hPa. The for the  
VOM-AoB2015. The variable atmospheric pressure was included in the VOM-AoB2015 and the model was optimized  
here for the period 1-1-1980 until 31-12-2005, due to the available time series from 1-1-1980. This was performed to  
assess the importance of precise atmospheric pressure data for the VOM simulations.

– 6. Optimized grass rooting depth ~~the~~

The rooting depth of grasses was prescribed at 1.0 m by Schymanski et al. (2009, 2015) in the VOM-AoB2015, which is  
325 roughly the position of a hard pan in the soil profile at Howard Springs. In this study the VOM-v0.5, grass rooting depth  
is optimized along with the tree rooting depth at each site separately. The model was optimized here in order to let also  
the grass rooting depths adapt to local conditions. To assess the effect of an optimized grass rooting depth separately, we  
also optimized it in the VOM-AoB2015 simulations for the period 1-1-1976 until 31-12-2005.

– 7. Updated meteorological data ~~a~~

A new version of the meteorological data from the Australian SILO Data Drill (Jeffrey et al., 2001) was used in the  
330 VOM-v0.5, starting from 1-1-1980. Therefore, the model was optimized here VOM-AoB2015 was also optimized with  
the new meteorological data, for the period 1-1-1980 until 31-12-2005. The time series of daily maximum and minimum  
temperatures, shortwave radiation, precipitation, vapour pressure and atmospheric pressure were all updated, but the  
CO<sub>2</sub>-concentrations kept fixed at 350 ppm. In this way, it can be assessed to what extent the different data versions lead  
to different model results.

– 8. Updated and extended meteorological data :~~the~~

The new version of the meteorological data from the Australian SILO Data Drill (Jeffrey et al., 2001) ~~covers also~~ includes more recent years, ~~which were included in the VOM-v0.5 simulations. To find out in how far the inclusion of more recent meteorological forcing alone affected the results, we also re-ran the VOM-AoB2015 with the extended meteorological forcing but constant atmospheric CO<sub>2</sub>-concentration of 350 ppm. Therefore, the model period of the VOM-AoB2015 was extended and the model was optimized from 1-1-1980 until 31-12-2017. The time series of daily maximum and minimum temperatures, shortwave radiation, precipitation, vapour pressure and atmospheric pressure were all updated, but the CO<sub>2</sub>-concentrations kept fixed at 350 ppm.~~

340

– Modified hydrology: in order to simulate 9. Modified hydrology

In the VOM-AoB2015, the average slope of the seepage face  $\gamma_0$  and hydrological length scale  $\Lambda_s$  were adopted from Reggiani et al. (2000) and set to 0.033 rad and 10 m, respectively, in absence of more detailed knowledge about these parameters. At the same time, the drainage level  $z_r$  and total soil thickness  $c_z$  were set to 10 m and 15 m, respectively, based on the local topography around the flux tower site (Schymanski et al., 2008b). This hydrological schematization resulted in groundwater tables around 5 m below the surface.

350

The hydrological parameters for the VOM-v0.5 were set in a way to resemble freely draining conditions ~~over the transect, in accordance with model simulations reported by Whitley et al. (2016), the position of drainage channels was set to~~, i.e. avoiding a significant influence of groundwater in Figure 2, required for a systematic comparison with other model applications in the accompanying paper of Nijzink et al. (2021), with a total soil thickness  $c_z$  of 30 m, a fast drainage parameterization with a drainage level  $z_r$  of 5 m (i.e. 25 m below the surface ~~and drainage parameters were set in a way to not let groundwater rise significantly above this (see also sect 2.2.5). The model was optimized here~~), a length scale for seepage outflow  $\Lambda_s$  set to 2 m and a channel slope  $\gamma_0$  set to 0.02 rad.

355

Therefore, the VOM-AoB2015 was optimized with the new hydrological schematization of the VOM-v0.5 for the period 1-1-1976 until 31-12-2005. ~~In this way, the effect of the hydrological settings on the model results can be assessed.~~

360

– 10. Modified soil properties : ~~To improve realism, physical soil properties were not assumed to be vertically homogeneous, but varied with 20 cm depth increments (Table 2). Soil textures in the top 10 cm were~~

The soils were assumed vertically homogeneous in the VOM-AoB2015, but were parameterized in the VOM-v0.5 based on field measurements of sand, clay and silt content provided by L. B. Hutley and J. Beringer, ~~whereas the soil textures in the top 10 cm, and the Soil and Landscape Grid of Australia (Viscarra Rossel et al., 2014a,b,c) for the deeper soil layers were based on data from the Soil and Landscape Grid of Australia (Viscarra Rossel et al., 2014a,b,e)~~ layers. The soils were classified into one of the soil textural groups of Carsel and Parrish (1988) based on the fractions of sand, silt and clay. Eventually, the parameters for the soil water retention model of Van Genuchten (1980) and the hydraulic conductivity were taken from the accompanying tables<sup>6</sup> from Carsel and Parrish (1988). See also Table 2 for

<sup>6</sup>see also <https://vom.readthedocs.io/en/latest/soildata.html>

the soil parameterization in the VOM-v0.5. As a result, the soil profile at Howard Springs is now assumed to consist of sandy loam in the top 0.4 m and sandy clay loam below, whereas Schymanski et al. (2015) assumed the soil to be VOM-AoB2015 used a soil of sandy loam in the entire soil profile. The model

The VOM-AoB2015 was optimized here with a modified soil profile, using the soil discretization of the VOM-AoB2015 of 0.5 m, with a sandy loam structure in the top layer and sandy clay loam below. This was done for the period 1-1-1976 until 31-12-2005, in order to assess the changes due to the different soils.

375 – 11. Modified soil properties and hydrology :the

The modified soils and hydrology, as described above, will strongly interact. For that reason, their combined effect was assessed by implementing both changes in the set-up of Schymanski et al. (2015). Free draining conditions are expected to reduce soil water storage, while finer soil texture is expected to increase water storage. In order to better understand in how far these changes compensated for each other, they were both implemented together in the VOM-AoB2015, while keeping everything else constant unmodified.

380 – 12. VOM-v0.5

Eventually, all changes were applied to the VOM-AoB2015, resulting in the new VOM-v0.5 simulations, as presented in the accompanying paper by Nijzink et al. (2021).

### 3 Results and Discussion

385 3.1 Effects of modifications to the VOM

To compare previous simulations using the VOM (Schymanski et al., 2015) with the new VOM-VOM-AoB2015 with the VOM-v0.5 set-up that includes the modifications as outlined in Sect. 2.2.9, each modification was applied to the previous setup in a stepwise manner one-step-at-a-time approach to quantify the influence of each change in isolation. The resulting simulations were compared with those presented in Schymanski et al. (2015) for the site Howard Springs. In general, sensitivities varied between +20% and -25% in total GPP and ET after optimizing the VOM with the new changes, and are summarized in Figure 3. Without optimizing the VOM, but still including the modifications, the sensitivities in GPP and ET were even smaller (see Supplement S1, Figure S1.51), except for a strong increase in soil evaporation after changing the soils. See also Supplement S1 for detailed time series.

The updated meteorological input data, for the runs until 31-12-2005 as well as the extended runs until 31-12-2017, hardly influenced the outcomes, with less than As expected, re-running the VOM-AoB2015 with the originally optimized parameters resulted in negligible differences. Re-running the optimization did result in slightly different results (12.6% higher projective cover for the perennials), but none of the simulated fluxes changed by more than 10% relative change in the resulting fluxes (Figure 3a and b). However, a higher contribution of the perennial vegetation in the fluxes can be observed, related to an

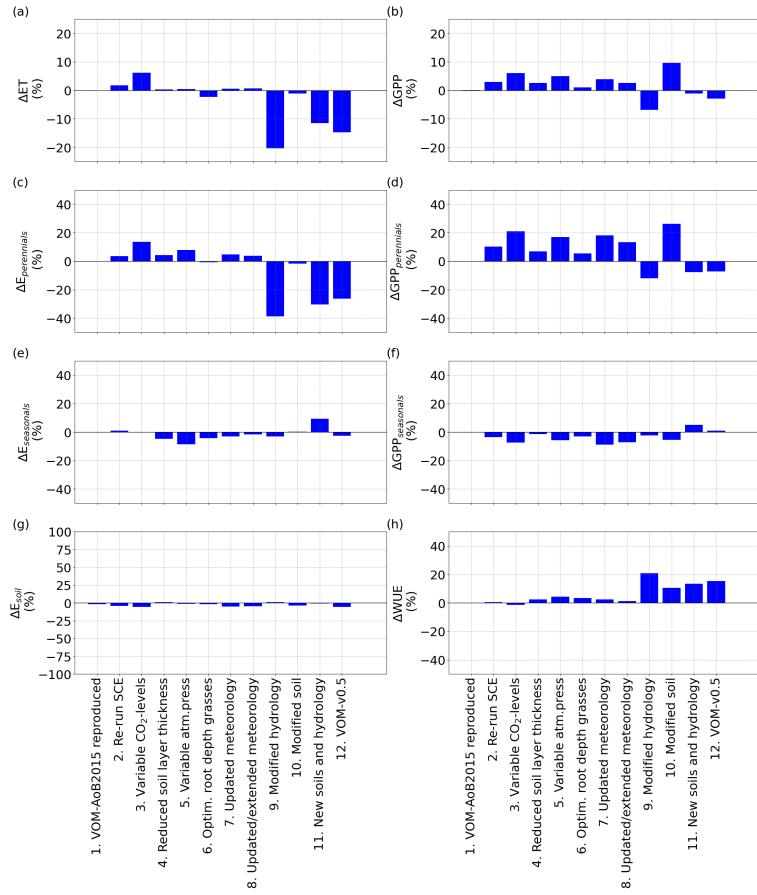


**Figure 3.** Relative changes in the mean annual values of the fluxes for the different (incremental) changes, as described in sect. 2.2.9, in comparison with [Sehymanski et al. \(2015\)](#) the VOM-AoB2015, with for a) mean annual-ET, b) mean annual-GPP, c) transpiration perennials (trees), d) mean annual-GPP perennials (trees), e) mean annual-transpiration seasonals (grasses), f) mean annual-GPP seasonals (grasses), g) mean annual-soil evaporation, and h) mean annual seepage face flow (Q<sub>sf</sub>), i) projected cover perennials (trees), j) projected cover seasonals (grasses), k) root depth perennials combined water use efficiency (trees WUE) of seasonal and l) root depth seasonals (grasses) perennial vegetation.

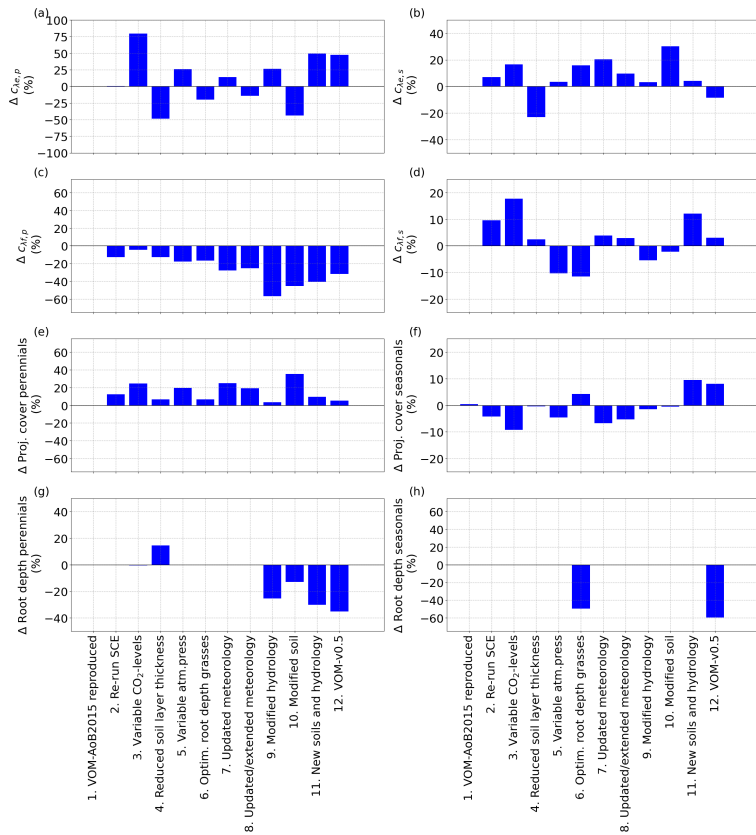


**Figure 4. Comparison between the results of Sehymanski et al. (2015) and VOM-AoB2015.** Relative changes in green, simulations using new soil and hydrological parameterization the vegetation properties for the different (red) incremental, and simulations using all changes, as described in combination (black) sect. 2.2.9, in comparison with the VOM-AoB2015, for a) ET the water use parameter  $c_{\lambda e,p}$  for perennial vegetation, b) transpiration by perennials (trees) the water use parameter  $c_{\lambda e,s}$  for seasonal vegetation, c) transpiration seasonal (grasses) the water use parameter  $c_{\lambda f,p}$  for perennial vegetation, d) soil evaporation the water use parameter  $c_{\lambda f,s}$  for seasonal vegetation, e) GPP, f) GPP projected cover perennials (trees), g) GPP mean projected cover seasonal (grasses), and hg) projective cover. Time series in a root depth perennials (trees) - and h) were smoothed using a moving average of 7 days. The daily average quality flags of the flux-tower observations are shown as a dashed line in Panel root depth seasonal (grasses), with a value of 100 for a completely gap-filled day and 1 for gap-free observations.

**Table 3.** Vegetation properties in the Vegetation Optimality Model optimized for maximizing the [Net-Carbon-ProfitNCP](#).

Parameter	Description	Initial range	Timescale	Unit
$c_{\lambda f,p}$	water use parameter perennial vegetation	0.0 - 10000.0	Long-term	$\text{mol mol}^{-1} \text{m}^{-1}$
$c_{\lambda e,p}$	water use parameter perennial vegetation	-3.0 - 0.0	Long-term	-
$c_{\lambda f,s}$	water use parameter seasonal vegetation	0.0 - 10000.0	Long-term	$\text{mol mol}^{-1} \text{m}^{-1}$
$c_{\lambda e,s}$	water use parameter seasonal vegetation	-3.0 - 0.0	Long-term	-
$M_{A,p}$	fractional cover perennial vegetation	0 - 1	Long-term	-
$y_{r,p}$	rooting depth perennial vegetation	1.0 - 9.0	Long-term	m
$y_{r,s}$	rooting depth seasonal vegetation	0.05 - 2	Long-term	m
$M_{A,s}$	fractional cover seasonal vegetation	0.00 - (1.0 - $\text{pet}$ $M_{A,p}$ )	Daily	-
$J_{max25,p}$	electron transport capacity perennial vegetation	-	Daily	$\text{mol s}^{-1} \text{m}^{-2}$
$J_{max25,s}$	electron transport capacity annual vegetation	-	Daily	$\text{mol s}^{-1} \text{m}^{-2}$
$G_{s,p}$	stomatal conductance perennial vegetation	-	Daily	$\text{mol s}^{-1} \text{m}^{-2}$
$G_{s,s}$	stomatal conductance seasonal vegetation	-	Daily	$\text{mol s}^{-1} \text{m}^{-2}$
$S_{Adr,i,s}$ $S_{Adr,i,p}$	root surface area distribution of perennial vegetation	-	Daily	$\text{m}^2 \text{m}^{-3}$
$S_{Adr,i,s}$	root surface area distribution of annual vegetation	-	Daily	$\text{m}^2 \text{m}^{-3}$

**Table 4.** [Modifications to the VOM-AoB2015](#).

Case	Base model	Modification	Model period
1. Reproduction VOM-AoB2015	VOM-AoB2015	None	1-1-1976 – 31-12-2005
2. Re-run SCE VOM-AoB2015	VOM-AoB2015	None	1-1-1976 – 31-12-2005
3. Variable CO <sub>2</sub> -levels	VOM-AoB2015	Constant CO <sub>2</sub> to variable	1-1-1976 – 31-12-2005
4. Reduced soil layer thickness	VOM-AoB2015	Soil layers from 0.5 m to 0.2 m	1-1-1976 – 31-12-2005
5. Variable atmospheric pressure	VOM-AoB2015	Constant pressure of 1013 hPa to variable	1-1-1980 – 31-12-2005
6. Optimized grass rooting depth	VOM-AoB2015	Grass roots from 1 m to optimized	1-1-1976 – 31-12-2005
7. Updated meteorological data	VOM-AoB2015	New SILO-data (Jeffrey et al., 2001)	1-1-1980 – 31-12-2005
8. Updated/extended meteorological data	VOM-AoB2015	New/extended SILO-data (Jeffrey et al., 2001)	1-1-1980 – 31-12-2017
9. Modified hydrology	VOM-AoB2015	New hydrological schematization	1-1-1976 – 31-12-2005
10. Modified soils	VOM-AoB2015	Update soil profiles	1-1-1976 – 31-12-2005
11. Modified soils and hydrology	VOM-AoB2015	New hydrological schematization and soils	1-1-1976 – 31-12-2005
12. VOM-v0.5	VOM-v0.5	All modifications included	1-1-1980 – 31-12-2017

increase in perennial vegetation cover (Figure 3i). This happened as well for re-running the SCE-algorithm, pointing at a 400 relatively large uncertainty in the predicted perennial cover, with a range of values that results in similar fluxes. % (Fig. 3).

405 ~~Changing In contrast, changing the fixed atmospheric CO<sub>2</sub>-levels (350 ppm) in the set-up of Schymanski et al. (2015)-VOM-AoB2015 to variable atmospheric CO<sub>2</sub>-levels had a relatively large influence on perennial vegetation, yielding values of GPP for perennial vegetation that were up to 21.0% higher (Figure 3d). Note that the CO<sub>2</sub>-levels of the Mauna Loa records have a mean of 369 ppm and a maximum of 410 ppm during the modelling period, i.e. mostly higher than the 350 ppm prescribed in Schymanski et al. (2015), who also simulated an increase in GPP by perennial plants in response to elevated CO<sub>2</sub>the VOM-AoB2015. See Figure S3.1f in Supplement S3 for more details about the CO<sub>2</sub>-levels used here.~~

410 Changing the vertical soil discretization of 0.5 m in Schymanski et al. (2015) the VOM-AoB2015 to a finer resolution of 0.2 m had a minor influence, with a change of less than the variability due to re-running the optimization algorithm (i.e. 2.6 % in the resulting GPP and 0.3 % in ET, Figure 3b, a). The variable atmospheric pressures only had a minor influence as well (5.0 % change in GPP and 0.4 % change in ET), which could also relate to re-running the optimization algorithm.

415 Similarly, when the grass rooting depths were optimized instead of the prescribed grass rooting prescribed to a depth of 1 m (everything else being the same as in Schymanski et al. (2015)), simulated GPP and ET were changed by 1.0% and -2.3% respectively (Figure 3b and a). The optimization led to shallower grass roots of 0.5 m (incurring lower carbon costs) and therefore to reductions in GPP and ET.

420 415 Stronger effects were found for the updated soil texture, which resulted in slightly reduced ET (-1.5%) but clearly increased GPP by 9.5%. The updated meteorological input data, for the runs until 31-12-2005 as well as the extended runs until 31-12-2017, hardly influenced the outcomes, with less than 10% relative change in the resulting fluxes (Figure 3a and b). The reduction in ET for an updated soil texture was mainly due to a large reduction in transpiration by seasonal vegetation. At the same time, simulated soil evaporation was increased, relating to an increased soil water storage and pointing at a reduced ability of the roots to take up water due to reduced hydraulic conductivity in the soil. The increase in simulated GPP was largely due to increased GPP by perennial vegetation, which at the same time slightly increased its transpiration. These changes were connected to a largely increased However, a higher contribution of the perennial vegetation in the fluxes can be observed, related to an increase in perennial vegetation cover and reduced rooting depth compared to the original simulations (vegetation cover went up to 0.51 from 0.31, while rooting depth went down to 3.5 m from 4 m). Overall, the perennial vegetation benefited from the finer soil texture due to larger soil moisture storage capacity and carry over of soil moisture into the dry season, whereas the seasonal vegetation suffered from reduced root water uptake due to lower hydraulic conductivity and increased soil evaporation during the wet season (Figure 4e). This happened as well for re-running the SCE-algorithm, and the changes related to the updated meteorological input could be attributed to re-running the optimization algorithm as well.

425 The implementation of free draining conditions had strong effects on the simulated fluxes as well, with lower values of both ET and GPP (-20.4% and -6.9% respectively, Figure 3a and b). However, here especially the simulated ET transpiration of perennial vegetation was reduced, whereas the transpiration by seasonal vegetation stayed relatively similar (Figure 3c and e). This is because in the original simulations, capillary rise from the water table was most important during the dry season, when

seasonal vegetation is inactive, and a change in the water table due to free draining conditions affects therefore mostly the perennial and not so much the seasonal vegetation.

435 Even stronger effects were found for the updated soil texture, which resulted in slightly reduced ET (-1.1%), but clearly increased GPP by 9.6% (Figure 3a and b). The increase in simulated GPP was largely due to increased GPP by perennial vegetation, which at the same time slightly decreased its transpiration. These changes were connected to a largely increased perennial vegetation cover and reduced rooting depth compared to the original simulations (vegetation cover went up to 0.43 from 0.31, while rooting depth went down to 3.5 m from 4 m). Overall, the perennial vegetation benefited from the finer  
440 soil texture due to larger soil moisture storage capacity and carry-over of soil moisture into the dry season, which lead to higher suction heads in especially the lower layers (see also Supplement S1 Figure 1.40d). This compensated for the effects of increased resistivity due to lower values of the hydraulic conductivity, as can be observed from Supplement S1 Figure 1.41b, which indicates a clear reduction in transpiration of the perennial vegetation due to lower hydraulic conductivities. In contrast, the seasonal vegetation did not show large differences, relating to the same properties in the top layer (0- 0.5 m) as for the  
445 original VOM-AoB2015 set-up.

Combining the new soils with the new hydrological settings still resulted in a reduction in ET by -11.5%, whereas their combined effect on GPP led to only a small reduction by -1.1% (Figure 3a and b). Here, the reduction of ET occurred mainly during the wet-dry season, and related to reductions in the perennial transpiration (Figure 5a-c), whereas the GPP stayed relatively similar (Figure 5e).

450 These findings are in accordance with the isolated effects of the new soils and hydrology, where free drainage conditions resulted in a large reduction in ET and GPP, while finer soil texture resulted in a small reduction in ET but large increase in GPP. Hence, the finer soil texture largely compensated the effect on GPP, but not on ET.

The other changes had smaller effects on the fluxes, so we do not discuss them here individually. Instead, we will perform a more in-depth analysis of the differences in model results when all changes were combined. Besides the changes in the fluxes, 455 several changes in the optimized vegetation properties were observed as well (Figure 4 and Figure S1.49 in Supplement S1). Similar to the fluxes, the changes in vegetation parameters for reproducing VOM-AoB2015 and re-running the optimization algorithm remained small (Figure 4).

Interestingly, the implementation of variable CO<sub>2</sub>-concentrations led to a large increase in  $c_{\lambda_{\text{E},P}}$ , i.e. one of the water use strategy parameters of the perennials (Fig. 4a). Another effect was a larger perennial vegetation cover (Figure 4e), while the 460 seasonal cover was on average reduced, which relates to the generally elevated CO<sub>2</sub>-levels and the long-term optimization of the perennial vegetation cover. Hence, perennial vegetation cover benefited, and the grass cover, optimized on a daily basis, reduced on average (Figure 4f).

The reduced soil layer thickness mainly affected the water use parameters  $c_{\lambda_{\text{E},P}}$  and  $c_{\lambda_{\text{E},S}}$  (Figure 4a and b, respectively). At the same time, the root depths for the perennials increased (Figure 4g), which compensated for the change in water use, 465 resulting in only minor changes in the fluxes (Figure 3).

The variable atmospheric pressure led to changes in the vegetation parameters as well, but this stayed limited to a maximum of 25 % for  $c_{\lambda e,p}$  (Figure 4a). However, this is stronger than the observed changes in the resulting fluxes of ET and GPP (Figure 3), which remained much smaller, related also to the non-linear relationship between  $c_{\lambda}$ , ET and GPP.

Optimized grass rooting depths were strongly reduced compared to the prescribed 1 m, and this was accompanied by increased  $c_{\lambda e,s}$  and reduced  $c_{\lambda f,s}$  (Figure 4b and d), pointing at a more efficient water use strategy with less water transpired per assimilated CO<sub>2</sub> (Figure 3h).

The updated meteorology, as well as the updated and extended meteorology, led to changes in the vegetation properties as well. The projected cover for the perennials increased (24.8 %, Figure 4) from 31.7 % to 39.6 %, whereas the projected cover for the grasses decreased on average (-6.7 %, Figure 4). Also the water use strategy parameters (4a-d) changed, with especially a strong change for  $c_{\lambda f,p}$  with -27.8 % (Figure 4c), but the resulting total water use efficiency remained similar (Figure 3h).

The modified hydrology led to larger changes in the vegetation properties, with especially a strong decrease in  $c_{\lambda f,p}$  (Figure 4c), but as well for  $c_{\lambda f,s}$  (Figure 4d). Hence, the modified hydrology led to a more efficient water use (Figure 3h). At the same time, the root depths for the perennial trees strongly reduced as well (Figure 4g). The modified soils, in isolation, led to similar effects for the water use strategy parameters (Figure 4a-d), which resulted in a more efficient water use (Figure 3h), see also Supplement S1, Figure S1.38d). The projective cover of the perennial trees changed strongly increased by 60 % (Figure 4g), i.e. from 31.7 % to 50.8 %. In contrast, updating the soils and hydrology at the same time, resulted in a more moderate increase of the perennial vegetation cover (Figure 4e).

### 3.2 Resulting Comparing VOM-y0.5 and VOM-AoB2015: resulting differences and underlying mechanisms

After incorporating all the changes, the relative error for mean annual evapo-transpiration (ET) changed from an overestimation by 8.4% to an underestimation of -10.2%, whereas the relative error for the mean annual GPP changed from 17.8% to 14.7%.

The ensemble years in Figure 6 revealed that the evapo-transpiration (ET) was most strongly underestimated by the VOM during the dry season at Howard Springs. The observed groundwater tables (Figure 7a) ranged from 5-15 m depth seasonally, whereas the VOM was parameterized now to keep groundwater tables close to 25 m depth, ~~for consistence with free drainage conditions in other models~~ required for the accompanying paper of Nijzink et al. (2021). Schymanski et al. (2015) originally assumed a much shallower drainage level at Howard Springs, which led to groundwater tables around 5 meters depth, and better correspondence with the observed fluxes (Fig. 6).

The simulated soil moisture in the top soil layer, as illustrated in Fig. 7b, remained similar to the soil moisture values of Schymanski et al. (2015). The higher vertical resolution in the new model runs (20 cm cf. 50 cm soil layers) resulted in stronger surface soil moisture spikes around rainfall events, which makes the red line appear generally more noisy than the green line in Fig. 7b. Observed soil moisture in the upper 5 cm was generally lower than the simulated soil moisture in the top soil layer, particularly in the wet season. The total water storage in the ~~top 5 m of the soil profile was substantially higher (up to 5-fold)~~ root zone was generally higher during the dry season in the new model simulations compared to Schymanski et al. (2015) (Figure 7c), ~~but lower during the wet season~~. The water retention curves (Figure 8) also show a clear shift, especially for the layers below 0.4 m, indicating extra storage.

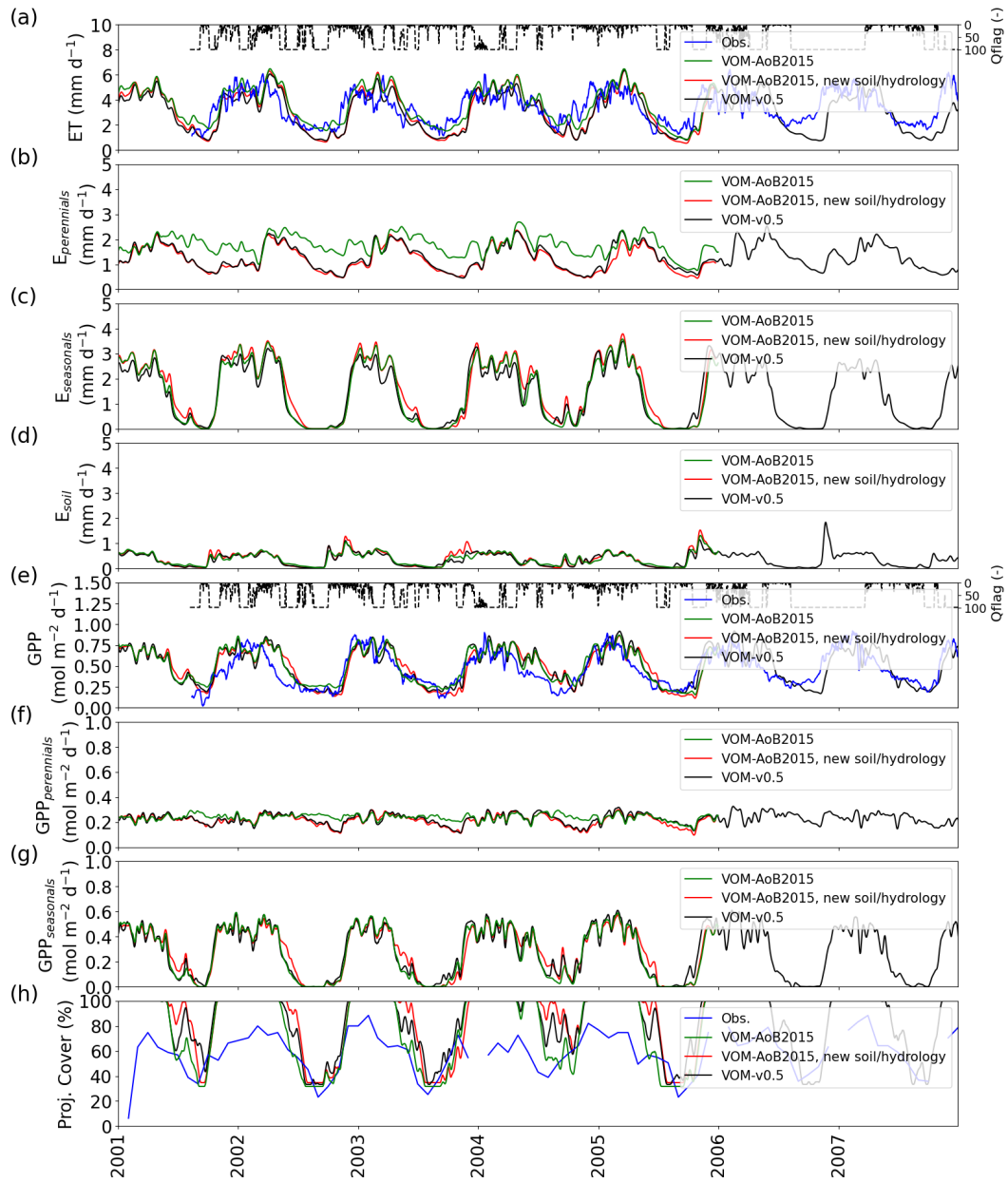


**Figure 5. Ensemble years** Comparison between the results of evapo-transpiration (the VOM-AoB2015 in green, simulations using new soil and hydrological parameterization (ET red), and gross primary productivity simulations using all changes in combination (GPP black) for the VOM. a) ET, b) transpiration by perennials (dark green trees), flux tower observations c) transpiration seasonal (black grasses), results of Schymanski et al. (2015) d) soil evaporation, e) GPP, f) GPP perennials (light green trees), all g) GPP seasonal (grasses), and h) projective cover. Time series in a)-g) were smoothed by using a 7-day moving average of 7 days. The ensemble years are calculated for the overlapping time periods with daily average quality flags of the flux tower observations are shown as a dashed line in Panel (7-8-2001 until 21-12-2006e), with a value of 100 for a completely gap-filled day and 1 for gap-free observations.

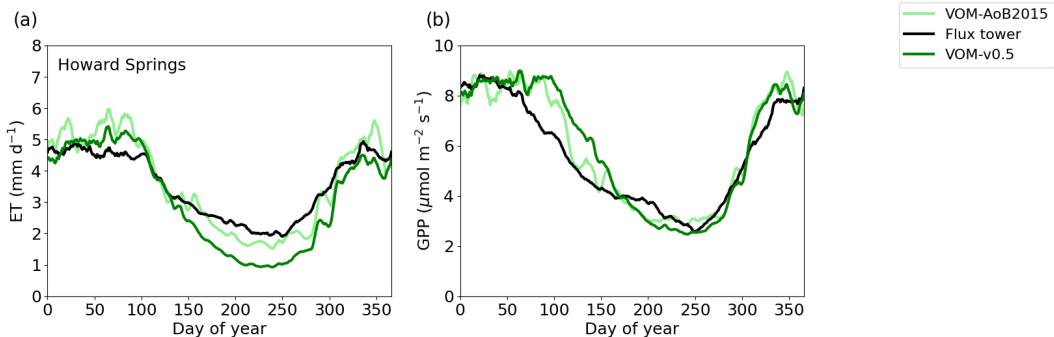


**Figure 6.** Ensemble years of evapo-transpiration (ET) and gross primary productivity (GPP) for the VOM-v0.5 (dark green), flux tower observations (black) and VOM-AoB2015 (light green), all smoothed by a 7-day moving average. The ensemble years are calculated for the overlapping time periods with the flux tower observations (7-8-2001 until 21-12-2016).

500 However, the water ~~potentials-suction heads~~ again showed strong similarities between the current model runs and the results of Schymanski et al. (2015) (Figures 7d and e, respectively), ~~but~~ with differences reflecting the vertical resolutions of the soil domains and simulated rooting depths, ~~and generally higher values for the VOM-v0.5 for the deeper layers. Hence, the water holding capacity increased for the deeper layers, but resistivity increased as well due to lower hydraulic conductivities. Changing the hydraulic conductivity in isolation, clearly leads to reductions in ET for the perennials (Supplement S1, Figure 505 S1.41b) due to the increased resistivity. Nevertheless, this is in the final VOM-v0.5 compensated for by the newly optimized water use strategy parameters. However, the new soil structure has the largest effect, as can be observed when running the VOM-v0.5 (i.e. with the new soils) with the water use strategy parameters of the VOM-AoB2015 in Figure S1.56b of Supplement S1.~~

#### 4 Conclusions

510 ~~The~~ As models, input data and parameterizations evolve, the effects of individual improvements are usually not systematically evaluated. Here, we analyse the effects of changes to the Vegetation Optimality Model ~~has undergone several changes regarding model set-up and input data since its last application by Schymanski et al. (2015) (VOM) between version VOM-AoB2015 and VOM-v0.5, the latter of which is the basis of a companion paper (Nijzink et al., 2021)). Some of the modifications were done for improved realism, while others for better comparability with other models and general applicability across the different sites investigated.~~

515 The modifications consisted of updated and extended input data, the use of variable atmospheric CO<sub>2</sub>-levels, modified soil properties, modified drainage levels as well as the addition of grass rooting depths to the optimized vegetation properties. The changes were applied to the VOM in a ~~step-wise manner~~ one-step manner for the flux tower site Howard Springs, by applying

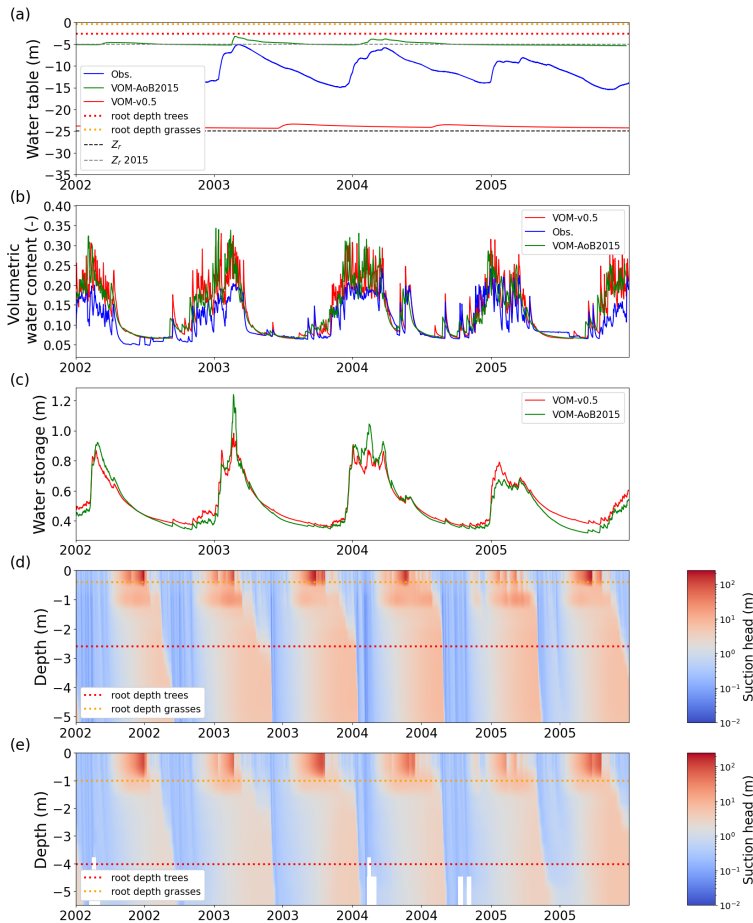


**Figure 7.** Simulated and observed hydrological state variables at Howard Springs. (a) groundwater depths, with dashed lines representing the prescribed bedrock depths, dotted lines the rooting depths (trees in red and grasses in orange), the [VOM-results](#) [VOM-v0.5](#) in red, the [results of Schymanski et al. \(2015\)](#) [VOM-AoB2015](#) in green, and observations of three different bore holes in the vicinity of the study site in blue (Northern Territory Government, Australia, 2018); (b) the volumetric water content in the upper soil layer with the VOM results in red, the results of Schymanski et al. (2015) in green and measurement-based values at 5 cm depth at the flux tower sites in blue; (c) the total water storage in the [upper 5 m root zone](#) for the [VOM-VOM-v0.5](#) (red, [storage until 2.6 m](#)) and the [results of Schymanski et al. \(2015\)-VOM-AoB2015](#) in green ([storage until 4.0 m](#)); (d) the [matrix water potentials suction heads](#) for the [current model runs of the VOMVOM-v0.5](#); and (e) the [matrix water potentials suction heads](#) of [Sehymanski et al. \(2015\)](#) [the VOM-AoB2015](#). Observed water tables in Panel a) were obtained from the Water data portal, (Northern Territory Government, Australia, 2018, accessed 8-3-2019).

each modification to the previous set-up of Schymanski et al. (2015) in isolation to evaluate its effect on the results, before  
520 combining all modifications and analyzing their effect in combination.

This analysis revealed that updated soil textures and a changed hydrological schematization had a strong influence on the results. An underestimation of dry season ET at Howard Springs was much more apparent when compared to the results of

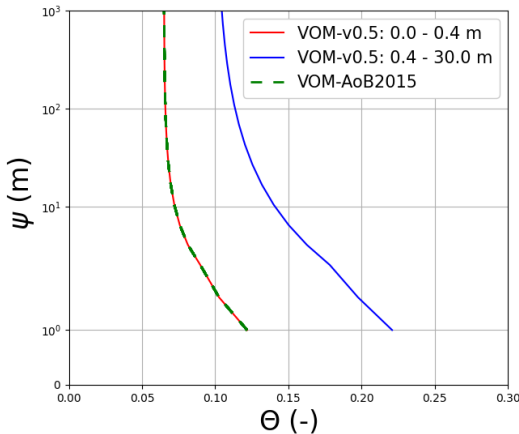


**Figure 8.** Water retention curves at Howard Springs for the ~~current VOM results~~ VOM-v0.5 results (red: top two layers, blue: deeper layers), and the results of ~~Schymanski et al. (2015)~~ the VOM-AoB2015 in green. Note that multiple red lines are shown ~~for the VOM-v0.5~~ due to the different soil parameterizations per soil layer in the current model runs, whereas ~~Schymanski et al. (2015)~~ the VOM-AoB2015 used one soil parameterization for all soil layers. The upper soil layers have however the same soil parameters, leading to overlapping curves (red and dashed green).

Schymanski et al. (2015), where the drainage parameterization maintained a water table depth much closer to the observed water table at this site. The effect of a much deeper groundwater table in the present simulations was partly buffered by a more  
 525 fine-grained soil texture below 0.4 m (sandy clay loam instead of sandy loam), which resulted in an increase in ~~water storage~~  
~~at otherwise similar water potentials in the top 5 m of soil~~ field capacities in the deeper soil layers compared to the simulations  
 by Schymanski et al. (2015). The use of variable atmospheric CO<sub>2</sub>-levels also had a strong influence on the results, which is  
 especially important as the model time period has been extended in this study. This was mainly due to generally higher levels  
 of atmospheric CO<sub>2</sub> in recent observations, compared to the constant values used by Schymanski et al. (2015).

530 ~~The stepwise analysis of modifications to a model setup and comparison against a benchmark dataset proved very helpful for identifying sensitivities of simulations to the different changes that might otherwise remain undiscovered due to compensating effects of the various modifications during model development. In this way, we found~~ Hence, our approach led to the insights that the neglect of a varying water table may have a strong effect on simulated surface fluxes, especially when soils are highly  
 535 permeable. ~~This is in line with other studies (e.g. York et al., 2002; Bierkens and van den Hurk, 2007; Maxwell et al., 2007)~~  
~~, and shows that the~~ common assumption of free draining conditions in modelling studies should be revised, ~~and if such an~~  
~~. Interestingly, the deficiencies in TBMs related to water access and tree rooting depth as identified by Whitley et al. (2016)~~  
~~strongly relate to this, as root depths also depend on groundwater tables. At least, if a free draining~~ assumption is necessary,  
 due to a lack of better hydrological understanding of a given site, or for comparison with other model simulations ~~using this~~  
~~assumption (e.g. Whitley et al., 2016)~~, i.e. for the study in the accompanying paper of Nijzink et al. (2021), potential bias in  
 540 simulation results has to be acknowledged.

545 In addition to this, we can more generally conclude that optimality-based modelling is able to provide robust modelling results. The sensitivities for the different changes remained rather limited and varied only between +20% and -25% in total GPP and ET after re-optimizing, but implementing the changes without re-optimizing the vegetation properties, resulted in even smaller changes. Therefore, we gained confidence that the VOM will also provide reliable and robust results for other study sites along the North Australian Tropical Transect, with similar boundary conditions. At the same time, the new boundary conditions made the VOM comparable to the other TBMs of Whitley et al. (2016).

550 To conclude, with our analysis we identified more conceptual issues, e.g. the influence of the hydrological schematization, but also found confirmation that the optimality-based modelling approach provides a robust result. Our method is in line with other developments in terrestrial biosphere modelling, where benchmark testing is seen as a necessary step in the modelling process (Blyth et al., 2011; Abramowitz, 2012; Clark et al., 2021). Here, we provided an example on how to perform a systematic benchmark test in a one-step-at-a-time approach, i.e. applying one change in isolation to the benchmark model. This analysis of modifications to a model setup and comparison against a benchmark dataset proved very helpful for identifying sensitivities of simulations to the different changes that might otherwise remain undiscovered due to compensating effects of the various modifications during model development. Our work also highlights the importance of open source code and data. 555 The availability of the original VOM-AoB2015 code was a pre-requisite of conducting this analysis. The long-term storage of the new VOM-v0.5, all input data, parameterization and data analysis workflows used in the present study will ensure that the effects of future modifications can again be compared step-by-step to the results presented here. This is a pre-requisite for maintaining generality of a model, as opposed to models that are highly customized for a particular site and hence unable to provide general insights.

560 *Code and data availability.* Model code is available on github (<https://github.com/schymans/VOM>), release v0.5 is used in this study (<http://doi.org/10.5281/zenodo.3630081>). The full analysis including all scripts and data are available on renku (<https://renkulab.io/gitlab/remko.nijzink/vomcases>). Before final publication, static versions of these repositories will be uploaded to zenodo.org and receive a separate DOI.

565 *Author contributions.* SJS and RN designed the set-up of the study. Model code was originally developed by SJS, but updated and modified by RN. RN set-up the repositories for the pre-processing, modelling and post-processing on renkulab. LH and JB provided site-specific knowledge and data. The main manuscript and supplementary information were prepared by RN, together with input from SJS. LH and JB provided corrections, suggestions and textual inputs for the main manuscript.

*Competing interests.* The authors declare no conflict of interest

*Acknowledgements.* This study is part of the WAVE-project funded by the Luxembourg National Research Fund (FNR) ATTRACT programme (A16/SR/11254288).

570 This work used eddy covariance data collected by the TERN-OzFlux facility (<http://data.ozflux.org.au/portal/home>). OzFlux would like to acknowledge the financial support of the Australian Federal Government via the National Collaborative Research Infrastructure Scheme and the Education Investment Fund.

We acknowledge the SILO Data Drill hosted by the Queensland Department of Environment and Science for providing the meteorological data (<https://www.longpaddock.qld.gov.au/silo/>).

575 We acknowledge the Scripps CO<sub>2</sub> program ([https://scrippsco2.ucsd.edu/data/atmospheric\\_co2/primary\\_mlo\\_co2\\_record.html](https://scrippsco2.ucsd.edu/data/atmospheric_co2/primary_mlo_co2_record.html)) for the Mauna Loa Observatory Records.

We also acknowledge CSIRO for the Soil and Landscape Grid of Australia (<https://aclep.csiro.au/aclep/soilandlandscapegrid/index.html>) and the Australian monthly fPAR derived from Advanced Very High Resolution Radiometer reflectances - version 5 (<https://data.csiro.au/dap/landingpage?pid=csiro:6084>).

580 We acknowledge the Northern Territory Water Data WebPortal for the groundwater data (<https://water.nt.gov.au/>).

## References

Abramowitz, G.: Towards a public, standardized, diagnostic benchmarking system for land surface models, *Geoscientific Model Development*, 5, 819–827, <https://doi.org/10.5194/gmd-5-819-2012>, <https://www.geosci-model-dev.net/5/819/2012/>, 2012.

Allen, R. G., Pereira, L. S., Raes, D., and Smith, M.: Crop evapotranspiration - Guidelines for computing crop water requirements, *Irrigation and drainage paper 56*, FAO - Food and Agriculture Organization of the United Nations, Rome, 1998.

Asrar, G., Fuchs, M., Kanemasu, E. T., and Hatfield, J. L.: Estimating Absorbed Photosynthetic Radiation and Leaf Area Index from Spectral Reflectance in Wheat1, *Agronomy Journal*, 76, 300, <https://doi.org/10.2134/agronj1984.00021962007600020029x>, <https://www.agronomy.org/publications/aj/abstracts/76/2/AJ0760020300>, 1984.

Beringer, J., Hutley, L. B., McHugh, I., Arndt, S. K., Campbell, D., Cleugh, H. A., Cleverly, J., Resco de Dios, V., Eamus, D., Evans, B., Ewenz, C., Grace, P., Griebel, A., Haverd, V., Hinko-Najera, N., Huete, A., Isaac, P., Kanniah, K., Leuning, R., Liddell, M. J., Macfarlane, C., Meyer, W., Moore, C., Pendall, E., Phillips, A., Phillips, R. L., Prober, S. M., Restrepo-Coupe, N., Rutledge, S., Schroder, I., Silberstein, R., Southall, P., Yee, M. S., Tapper, N. J., van Gorsel, E., Vote, C., Walker, J., and Wardlaw, T.: An introduction to the Australian and New Zealand flux tower network –OzFlux, *Biogeosciences*, 13, 5895–5916, <https://doi.org/10.5194/bg-13-5895-2016>, <https://www.biogeosciences.net/13/5895/2016/>, 2016.

Beringer, J., McHugh, I., Hutley, L. B., Isaac, P., and Kljun, N.: Technical note: Dynamic INtegrated Gap-filling and partitioning for OzFlux (DINGO), *Biogeosciences*, 14, 1457–1460, <https://doi.org/10.5194/bg-14-1457-2017>, <https://www.biogeosciences.net/14/1457/2017/>, 2017.

Bierkens, M. F. P. and van den Hurk, B. J. J. M.: Groundwater convergence as a possible mechanism for multi-year persistence in rainfall, *Geophysical Research Letters*, 34, <https://doi.org/10.1029/2006GL028396>, <http://agupubs.onlinelibrary.wiley.com/doi/abs/10.1029/2006GL028396>, 2007.

Blyth, E., Clark, D. B., Ellis, R., Huntingford, C., Los, S., Pryor, M., Best, M., and Sitch, S.: A comprehensive set of benchmark tests for a land surface model of simultaneous fluxes of water and carbon at both the global and seasonal scale, *Geoscientific Model Development*, 4, 255–269, <https://doi.org/10.5194/gmd-4-255-2011>, <https://gmd.copernicus.org/articles/4/255/2011/>, 2011.

Buckley, T. N. and Roberts, D. W.: DESPOT, a process-based tree growth model that allocates carbon to maximize carbon gain, *Tree Physiology*, 26, 129–144, <https://doi.org/10.1093/treephys/26.2.129>, <https://academic.oup.com/treephys/article-lookup/doi/10.1093/treephys/26.2.129>, 2006.

Carsel, R. F. and Parrish, R. S.: Developing joint probability distributions of soil water retention characteristics, *Water Resources Research*, 24, 755–769, <https://doi.org/10.1029/WR024i005p00755>, <http://agupubs.onlinelibrary.wiley.com/doi/abs/10.1029/WR024i005p00755>, [\\_eprint: https://onlinelibrary.wiley.com/doi/pdf/10.1029/WR024i005p00755](http://onlinelibrary.wiley.com/doi/pdf/10.1029/WR024i005p00755), 1988.

Clark, M. P., Zolfaghari, R., Green, K. R., Trim, S., Knoben, W. J. M., Bennett, A., Nijssen, B., Ireson, A., and Spiteri, R. J.: The Numerical Implementation of Land Models: Problem Formulation and Laugh Tests, *Journal of Hydrometeorology*, 22, 1627–1648, <https://doi.org/10.1175/JHM-D-20-0175.1>, <https://journals.ametsoc.org/view/journals/hdr/aop/JHM-D-20-0175.1/JHM-D-20-0175.1.xml>, publisher: American Meteorological Society Section: Journal of Hydrometeorology, 2021.

Cowan, I. R. and Farquhar, G. D.: Stomatal Function in Relation to Leaf Metabolism and Environment, in: *Integration of activity in the higher plant*, edited by Jennings, D. H., pp. 471–505, Cambridge University Press, Cambridge, 1977.

Donohue, R., McVicar, T., and Roderick, M.: Australian monthly fPAR derived from Advanced Very High Resolution Radiometer reflectances - version 5. v1. CSIRO. Data Collection., <https://doi.org/10.4225/08/50FE0CBE0DD06>, 2013.

Donohue, R. J., Roderick, M. L., and McVicar, T. R.: Deriving consistent long-term vegetation information from AVHRR reflectance data using a cover-triangle-based framework, *Remote Sensing of Environment*, 112, 2938–2949, <https://doi.org/10.1016/j.rse.2008.02.008>, 620 <http://linkinghub.elsevier.com/retrieve/pii/S0034425708000618>, 2008.

Duan, Q., Sorooshian, S., and Gupta, V. K.: Optimal use of the SCE-UA global optimization method for calibrating watershed models, *Journal of Hydrology*, 158, 265–284, [https://doi.org/10.1016/0022-1694\(94\)90057-4](https://doi.org/10.1016/0022-1694(94)90057-4), <http://www.sciencedirect.com/science/article/pii/0022169494900574>, 1994.

Hikosaka, K.: A Model of Dynamics of Leaves and Nitrogen in a Plant Canopy: An Integration of Canopy Photosynthesis, Leaf Life Span, and Nitrogen Use Efficiency, *The American Naturalist*, 162, 149–164, <https://doi.org/10.1086/376576>, <https://www.journals.uchicago.edu/doi/10.1086/376576>, 2003.

Hutley, L. B.: Vegetation Above Ground Biomass, Litchfield Savanna SuperSite, Tower Plot, 2013, <https://supersites.tern.org.au/knb/metacat/supersite.118.6/html>, 2015.

Hutley, L. B., Beringer, J., Isaac, P. R., Hacker, J. M., and Cernusak, L. A.: A sub-continental scale living laboratory: Spatial patterns of savanna vegetation over a rainfall gradient in northern Australia, *Agricultural and Forest Meteorology*, 151, 1417–1428, 630 <https://doi.org/10.1016/j.agrformet.2011.03.002>, <http://www.sciencedirect.com/science/article/pii/S0168192311000839>, 2011.

Jeffrey, S. J., Carter, J. O., Moodie, K. B., and Beswick, A. R.: Using spatial interpolation to construct a comprehensive archive of Australian climate data, *Environmental Modelling & Software*, 16, 309–330, [https://doi.org/10.1016/S1364-8152\(01\)00008-1](https://doi.org/10.1016/S1364-8152(01)00008-1), <https://linkinghub.elsevier.com/retrieve/pii/S1364815201000081>, 2001.

Keeling, C. D., Piper, S. C., Bacastow, R. B., Wahlen, M., Whorf, T. P., Heimann, M., and Meijer, H. A.: Atmospheric CO<sub>2</sub> and 13CO<sub>2</sub> Exchange with the Terrestrial Biosphere and Oceans from 1978 to 2000: Observations and Carbon Cycle Implications, in: *A History of Atmospheric CO<sub>2</sub> and its effects on Plants, Animals, and Ecosystems*, pp. 83–113, Springer Verlag, New York, editors: Ehleringer, J.R., T. E. Cerling, M. D. Dearing, 2005.

Lu, H.: Decomposition of vegetation cover into woody and herbaceous components using AVHRR NDVI time series, *Remote Sensing of Environment*, 86, 1–18, [https://doi.org/10.1016/S0034-4257\(03\)00054-3](https://doi.org/10.1016/S0034-4257(03)00054-3), <https://linkinghub.elsevier.com/retrieve/pii/S0034425703000543>, 640 2003.

Ma, X., Huete, A., Yu, Q., Coupe, N. R., Davies, K., Broich, M., Ratana, P., Beringer, J., Hutley, L. B., Cleverly, J., Boulain, N., and Eamus, D.: Spatial patterns and temporal dynamics in savanna vegetation phenology across the North Australian Tropical Transect, *Remote Sensing of Environment*, 139, 97–115, <https://doi.org/10.1016/j.rse.2013.07.030>, <https://linkinghub.elsevier.com/retrieve/pii/S0034425713002423>, 2013.

Maxwell, R. M., Chow, F. K., and Kollet, S. J.: The groundwater–land-surface–atmosphere connection: Soil moisture effects on the atmospheric boundary layer in fully-coupled simulations, *Advances in Water Resources*, 30, 2447–2466, <https://doi.org/10.1016/j.advwatres.2007.05.018>, <https://linkinghub.elsevier.com/retrieve/pii/S0309170807000954>, 2007.

Nijzink, R. C., Beringer, J., Hutley, L. B., and Schymanski, S. J.: Does maximization of net carbon profit enable the prediction of vegetation behaviour in savanna sites along a precipitation gradient?, preprint, *Ecohydrology/Modelling approaches*, <https://doi.org/10.5194/hess-2021-265>, <https://hess.copernicus.org/preprints/hess-2021-265/>, 2021.

Northern Territory Government, Australia: Water data portal, <https://nt.gov.au/environment/water/water-information-systems/water-data-portal>, 2018.

Radcliffe, D. E. and Rasmussen, T. C.: Soil water movement, in: *Physics Companion*, pp. 85 – 126, CRC Press, Boca Raton, Fla, edited by 655 A.W. Warrick, 2002.

Raupach, M. R.: 19 Dynamics and Optimality in Coupled Terrestrial Energy, Water, Carbon and Nutrient Cycles, in: Predictions in Ungauged Basins: International Perspectives on State of the Art and Pathways Forward, p. 16, IAHS Press: Wallingford, 2005.

Reggiani, P., Sivapalan, M., and Hassanizadeh, S. M.: Conservation equations governing hillslope responses: Exploring the physical basis of water balance, *Water Resources Research*, 36, 1845–1863, <https://doi.org/10.1029/2000WR900066>, <http://doi.wiley.com/10.1029/2000WR900066>, 2000.

Rodríguez-Iturbe, I., D'Odorico, P., Porporato, A., and Ridolfi, L.: On the spatial and temporal links between vegetation, climate, and soil moisture, *Water Resources Research*, 35, 3709–3722, <https://doi.org/10.1029/1999WR900255>, <https://agupubs.onlinelibrary.wiley.com/doi/abs/10.1029/1999WR900255>, \_eprint: <https://agupubs.onlinelibrary.wiley.com/doi/pdf/10.1029/1999WR900255>, 1999.

Rodríguez-Iturbe, I., D'Odorico, P., Porporato, A., and Ridolfi, L.: Tree-grass coexistence in Savannas: The role of spatial dynamics and climate fluctuations, *Geophysical Research Letters*, 26, 247–250, <https://doi.org/10.1029/1998GL900296>, <https://agupubs.onlinelibrary.wiley.com/doi/abs/10.1029/1998GL900296>, \_eprint: <https://agupubs.onlinelibrary.wiley.com/doi/pdf/10.1029/1998GL900296>, 1999.

Savenije, H. H. G.: The importance of interception and why we should delete the term evapotranspiration from our vocabulary, *Hydrological Processes*, 18, 1507–1511, <https://doi.org/10.1002/hyp.5563>, <http://onlinelibrary.wiley.com/doi/abs/10.1002/hyp.5563>, \_eprint: <https://onlinelibrary.wiley.com/doi/pdf/10.1002/hyp.5563>, 2004.

Schenk, H. J. and Jackson, R. B.: Rooting depths, lateral root spreads and below-ground/above-ground allometries of plants in water-limited ecosystems, *Journal of Ecology*, 90, 480–494, 2002.

Schymanski, S. J., Roderick, M. L., Sivapalan, M., Hutley, L. B., and Beringer, J.: A test of the optimality approach to modelling canopy properties and CO<sub>2</sub> uptake by natural vegetation, *Plant, Cell & Environment*, 30, 1586–1598, <https://doi.org/10.1111/j.1365-3040.2007.01728.x>, <http://www.blackwell-synergy.com/doi/abs/10.1111/j.1365-3040.2007.01728.x>, 2007.

Schymanski, S. J., Roderick, M. L., Sivapalan, M., Hutley, L. B., and Beringer, J.: A canopy-scale test of the optimal water use hypothesis, *Plant Cell & Environment*, 31, 97–111, <https://doi.org/10.1111/j.1365-3040.2007.01740.x>, <http://www.blackwell-synergy.com/doi/abs/10.1111/j.1365-3040.2007.01740.x>, 2008a.

Schymanski, S. J., Sivapalan, M., Roderick, M. L., Beringer, J., and Hutley, L. B.: An optimality-based model of the coupled soil moisture and root dynamics, *Hydrology and Earth System Sciences*, 12, 913–932, <https://doi.org/10.5194/hess-12-913-2008>, <http://www.hydrol-earth-syst-sci.net/12/913/2008/>, 2008b.

Schymanski, S. J., Sivapalan, M., Roderick, M. L., Hutley, L. B., and Beringer, J.: An optimality-based model of the dynamic feedbacks between natural vegetation and the water balance, *Water Resources Research*, 45, <https://doi.org/10.1029/2008WR006841>, <https://agupubs.onlinelibrary-wiley-com.proxy.bnl.lu/doi/full/10.1029/2008WR006841>, 2009.

Schymanski, S. J., Roderick, M. L., and Sivapalan, M.: Using an optimality model to understand medium and long-term responses of vegetation water use to elevated atmospheric CO<sub>2</sub> concentrations, *AoB Plants*, 7, plv060, <https://doi.org/10.1093/aobpla/plv060>, <http://aobpla.oxfordjournals.org/content/7/plv060>, 2015.

Van Genuchten, M. T.: A Closed-form Equation for Predicting the Hydraulic Conductivity of Unsaturated Soils, *Soil Science Society of America Journal*, 44, 892–898, <https://doi.org/10.2136/sssaj1980.03615995004400050002x>, <http://acsess.onlinelibrary.wiley.com/doi/abs/10.2136/sssaj1980.03615995004400050002x>, \_eprint: <https://onlinelibrary.wiley.com/doi/pdf/10.2136/sssaj1980.03615995004400050002x>, 1980.

Viscarra Rossel, R., Chen, C., Grundy, M., Searle, R., Clifford, D., Odgers, N., Holmes, K., Griffin, T., Liddicoat, C., and Kidd, D.: Soil and Landscape Grid National Soil Attribute Maps - Clay (3" resolution) - Release 1, <https://doi.org/10.4225/08/546EEE35164BF>, <https://data.csiro.au/collections/#collection/CIcsiro:10168v5>, type: dataset, 2014a.

Viscarra Rossel, R., Chen, C., Grundy, M., Searle, R., Clifford, D., Odgers, N., Holmes, K., Griffin, T., Liddicoat, C., and Kidd, D.: Soil and Landscape Grid National Soil Attribute Maps - Silt (3" resolution) - Release 1, <https://doi.org/10.4225/08/546F48D6A6D48>, <https://data.csiro.au/collections/#collection/CIcsiro:10688v5>, type: dataset, 2014b.

Viscarra Rossel, R., Chen, C., Grundy, M., Searle, R., Clifford, D., Odgers, N., Holmes, K., Griffin, T., Liddicoat, C., and Kidd, D.: Soil and Landscape Grid National Soil Attribute Maps - Sand (3" resolution) - Release 1, <https://doi.org/10.4225/08/546F29646877E>, <https://data.csiro.au/collections/#collection/CIcsiro:10149v5>, type: dataset, 2014c.

700 von Caemmerer, S.: Biochemical Models of Leaf Photosynthesis, vol. 2 of *Techniques in Plant Sciences*, CSIRO Publishing, Collingwood, 2000.

Whitley, R., Beringer, J., Hutley, L. B., Abramowitz, G., De Kauwe, M. G., Duursma, R., Evans, B., Haverd, V., Li, L., Ryu, Y., Smith, B., Wang, Y.-P., Williams, M., and Yu, Q.: A model inter-comparison study to examine limiting factors in modelling Australian tropical savannas, *Biogeosciences*, 13, 3245–3265, <https://doi.org/10.5194/bg-13-3245-2016>, <http://www.biogeosciences.net/13/3245/2016/>, 2016.

705 Williams, R. J., Duff, G. A., Bowman, D. M. J. S., and Cook, G. D.: Variation in the composition and structure of tropical savannas as a function of rainfall and soil texture along a large-scale climatic gradient in the Northern Territory, Australia, *Journal of Biogeography*, 23, 747–756, <https://doi.org/10.1111/j.1365-2699.1996.tb00036.x>, <https://onlinelibrary.wiley.com/doi/abs/10.1111/j.1365-2699.1996.tb00036.x>, 1996.

710 York, J. P., Person, M., Gutowski, W. J., and Winter, T. C.: Putting aquifers into atmospheric simulation models: an example from the Mill Creek Watershed, northeastern Kansas, *Advances in Water Resources*, 25, 221–238, [https://doi.org/10.1016/S0309-1708\(01\)00021-5](https://doi.org/10.1016/S0309-1708(01)00021-5), <https://linkinghub.elsevier.com/retrieve/pii/S0309170801000215>, 2002.